CHALMERS
UNIVERSITY OF TECHNOLOGY

Parametric Lattices Are Better Quantizers in Dimensions 13 and 14

Downloaded from: https://research.chalmers.se, 2026-11-14 02:52 UTC

Citation for the original published paper (version of record):
Pook-Kolb, D., Agrell, E., Allen, B. (2026). Parametric Lattices Are Better Quantizers in Dimensions 13 and 14. IEEE Transactions on Information Theory, 72(11): 8909-8925.
http://dx.doi.org/10.1109/TIT.2026.3721285

N.B. When citing this work, cite the original published paper.

© 2026 IEEE. Personal use of this material is permitted. Permission from IEEE must be obtained for all other uses, in any current or future media, including reprinting/republishing this material for advertising or promotional purposes, or reuse of any copyrighted component of this work in other works.

(article starts on next page)

Parametric Lattices Are Better Quantizers in Dimensions 13 and 14

Daniel Pook-Kolb, Erik Agrell, *Fellow, IEEE*, and Bruce Allen, *Member, IEEE*

***Abstract*—New lattice quantizers with lower normalized second moments than previously reported are constructed in 13 and 14 dimensions and conjectured to be optimal. Our construction combines an initial numerical optimization with a subsequent analytical optimization of families of lattices, whose Voronoi regions are constructed exactly. The new lattices are constructed from glued products of previously known lattices, by scaling the component lattices and then optimizing the scale factors. A two-parameter family of lattices in 13 dimensions reveals an intricate landscape of phase changes as the parameters are varied.**

***Index Terms*—gluing theory, lattice design, lattice quantization, lattice theory, mean square error, moment of inertia, normalized second moment, parametric lattice, quantization constant, quantization error, theta image, vector quantization, Voronoi region.**

I. Introduction

THE *lattice quantizer* problem is to find a lattice with the minimal normalized second moment (NSM) in a given dimension [1, Ch. 2]. Geometrically, this minimizes the mean squared distance from a random point to the closest lattice point, when the number of lattice points per unit volume is fixed. It is one of the classical problems in lattice theory and has applications in fields ranging from constellation shaping [2], [3] and cryptography [4] to machine learning [5] and data analysis [6].

Above all, the interest in lattice quantization was fueled by progress in data compression [7], [8, Chs. 1, 3–5]. If multi-dimensional data drawn from a continuous source distribution is to be represented digitally, then the distribution needs to be approximated by a finite set of points, a *vector quantizer.* The quantization error, which is the mean square error between a random point drawn from the given distribution and its closest vector quantizer point, should be minimized. According to a well-known conjecture by Allen Gersho, the optimal vector quantizer with asymptotically many points has the property that all Voronoi regions are congruent to each other [9], which is a key feature of lattices.

Proofs of optimality of a lattice for quantization exist only in dimensions up to three. In two dimensions, the optimal lattice quantizer is the hexagonal lattice [10] and in three dimensions it is the body-centered cubic lattice [11]. Together with these proven results, the lattices with the lowest known normalized second moments in dimensions 4–8, 12, 16, and 24 were listed in 1984 by Conway and Sloane [12] and conjectured optimal by the same authors in 1999 [1, p. 13]. Remarkably, the conjectured optimal lattice quantizer in 12 dimensions, the Coxeter–Todd lattice K_{12}, is surpassed by lattices found in 2010 by Kudryashov and Yurkov [13] and rediscovered and analyzed by the present authors using a different construction technique [14]; see Appendix B-B.

In dimensions 13 and 14, the focus of the present paper, the best known lattice quantizers were for a long time the duals of the checkerboard lattice D_{13}^* and D_{14}^* [12, Fig. 2], [1, Fig. 2.9]. Both were surpassed by a product of K_{12} and a low-dimensional lattice [15]. Using a better quantizer than K_{12} in 12 dimensions gives a slightly improved product lattice in 13 dimensions [14]. A lamination of K_{12} led to a non-product lattice with an even lower NSM [16]. Lyu et al. obtained a better 14-dimensional lattice from a complex lattice over the Eisenstein integers in 2022 [17].

With one exception, the best known lattice quantizers are *integral lattices,* i.e., lattices such that the inner product between any pair of lattice vectors is an integer. The exception is in 9 dimensions, where a conjectured optimal lattice was found in 1998 by Agrell and Eriksson using numerical optimization [18]. It was defined using a 9×9 generator matrix, where 80 components are exact and one is "just a computer number," as the lattice pioneer Neil Sloane once commented [19]. It took until 2021 to identify the square of this "computer number" as the root of a ninth-order polynomial [20]. We call such lattices, which are exact functions of a small number of real parameters, *parametric lattices.*

The work reported here employs both numerical approximation methods and exact analytic ones. While this mixed approach to finding optimal lattice quantizers is decades old, there has been recent progress. In [21], numerical optimization was performed in dimensions 10–16 using an improved stochastic gradient descent method. This is complemented in the same work by a new identification technique to find exact lattices from approximate numerical representations. In all dimensions except 13, 14, and 15, the previously known lattices with the lowest normalized second moment were recovered, providing strong numerical evidence for the conjecture that these are the optimal lattice quantizers in their dimension. In dimension 15, the lattice Λ_{15}^*, i.e., the dual of the laminated lattice Λ_{15}, was identified and conjectured optimal. Results in the only remaining dimensions 13 and 14 were reported

The work of E. Agrell was supported by a Collaborating Scientist Grant from the Max Planck Institute for Gravitational Physics, Germany, which is gratefully acknowledged.

D. Pook-Kolb and B. Allen are with the Max Planck Institute for Gravitational Physics, 30167 Hannover, Germany, and Leibniz Universität Hannover (e-mail: daniel.pook.kolb@aei.mpg.de and bruce.allen@aei.mpg.de).

E. Agrell is with the Department of Electrical Engineering, Chalmers University of Technology, 41296 Gothenburg, Sweden (e-mail: agrell@chalmers.se).

This article has supplementary material provided by the authors and color versions of one or more figures available at https://doi.org/10.1109/TIT.2026.3721285.

numerically, with further analysis deferred to future work. That is the purpose of the present paper.

First, the lattices found numerically in dimensions 13 and 14 are identified using the technique described in [21]: solving systems of equations derived from their theta images. The technique does not return exact representations of these two lattices, but rather reveals them to be parametric lattices, somewhat similar to the best 9-dimensional one [20]. Then, by optimizing the parameters using the methods developed in [16], [20], we obtain exact lattice quantizers with the lowest normalized second moments reported in dimensions 13 and 14, and conjecture these lattices to be optimal in their dimensions.

II. Lattice Definitions

A. Basic notions

An n-dimensional lattice L in $\mathbb{R}^m$, $m \geq n$, is the set of all linear combinations of n linearly independent *basis vectors* in $\mathbb{R}^m$ with integer coefficients. With the convention that all vectors are row vectors, we can write

$$L \triangleq \{\boldsymbol{u}\boldsymbol{B} \colon \boldsymbol{u} \in \mathbb{Z}^n\}, \tag{1}$$

where $\boldsymbol{B}$ is an $n \times m$ *generator matrix* of L whose rows are the basis vectors. There are infinitely many generator matrices for the same lattice L.

The *dual lattice* L^* of a lattice L with generator matrix $\boldsymbol{B}$ is generated by the matrix $\boldsymbol{B}^* \triangleq \boldsymbol{A}^{-1}\boldsymbol{B}$, where $\boldsymbol{A} \triangleq \boldsymbol{B}\boldsymbol{B}^T$ is a *Gram matrix* of L. Similar to generator matrices, Gram matrices are not unique for a given lattice, but their determinants depend only on L [1, p. 4]. A lattice is an integral lattice if and only if its Gram matrix has only integer entries.

Two lattices L and L' are called *equivalent* if one can be transformed into the other by a combination of rotations, reflections, and/or changes of scale [1, p. 10]. This means that for any n-dimensional lattice L in $\mathbb{R}^m$, $m > n$, there exists an equivalent lattice L' in $\mathbb{R}^n$. When a lattice L is presented with nonsquare generator matrix $\boldsymbol{B}$, then this is often because $\boldsymbol{B}$ takes on a more elegant form making it easier to understand. However, since L is equivalent to a corresponding lattice in $\mathbb{R}^n$, i.e., with square $\boldsymbol{B}$, we henceforth assume that $m = n$ to simplify the discussion.[1] In that case, $\boldsymbol{B}^* = (\boldsymbol{B}^T)^{-1}$.

The *Voronoi region* of a lattice point $\boldsymbol{x} \in L$ is the set of all points in $\mathbb{R}^n$ closer to $\boldsymbol{x}$ than to any other lattice point. By definition, the origin $\boldsymbol{0}$ is always a lattice point, and we denote the Voronoi region of $\boldsymbol{0}$ by Ω. The volume of Ω is $V = \sqrt{\det \boldsymbol{A}} = |\det \boldsymbol{B}|$.

The lattice quantizer problem is to find a lattice L with the minimal NSM or *quantizer constant* [1, pp. 34, 56–62]

$$G(L) \triangleq \frac{1}{nV^{1+2/n}} \int_\Omega \|\boldsymbol{x}\|^2 \, \mathrm{d}\boldsymbol{x}. \tag{2}$$

The normalization by $1/V^{1+2/n}$ makes G independent of the lattice's scale, i.e., $G(L) = G(aL)$ for all $a > 0$. The factor of $1/n$ is a convention that ensures that the n-dimensional cubic lattice $\mathbb{Z}^n$ has the same NSM in all dimensions, with $G(\mathbb{Z}^n) = 1/12$. It also has the consequence that

$$G(L \times L) = G(L), \tag{3}$$

where $L \times L$ is a product lattice defined in Sec. II-B. If L and L' are equivalent lattices, then their respective NSMs are the same, $G(L) = G(L')$.

In 1996, Zamir and Feder [22] proved a useful necessary condition that a globally optimal lattice quantizer satisfies. Let $\boldsymbol{U}$ denote the *second moment matrix* of L defined by

$$\boldsymbol{U} \triangleq \frac{1}{V} \int_\Omega \boldsymbol{x}^T \boldsymbol{x} \, \mathrm{d}\boldsymbol{x}. \tag{4}$$

Then, if L is a globally optimal lattice quantizer, $\boldsymbol{U}$ is proportional to the n-dimensional identity matrix $\boldsymbol{I}_n$. This result is generalized in [15] to apply to *locally* optimal lattice quantizers as well. Note that this is only a necessary condition. If $\boldsymbol{U}$ is not proportional to the identity, then L is not even locally optimal. This will become an important point in our analysis, especially for the novel 13-dimensional lattice.

B. Product lattices

The Cartesian product of k lattices $L_1, \ldots, L_k$ is the set of row vectors

$$L^\times \triangleq L_1 \times \cdots \times L_k = \{[\boldsymbol{x}_1 \ \cdots \ \boldsymbol{x}_k] \colon \boldsymbol{x}_i \in L_i, i = 1, \ldots, k\}. \tag{5}$$

Let $a_1, \ldots, a_k$ be real, positive scale factors. Then

$$\bar{L}^\times \triangleq a_1 L_1 \times \cdots \times a_k L_k = \{[a_1\boldsymbol{x}_1 \ \cdots \ a_k\boldsymbol{x}_k] \colon \boldsymbol{x}_i \in L_i, \forall i\} \tag{6}$$

is called the *product lattice* of the scaled *component lattices* $L_1, \ldots, L_k$. It is a special case of a parametric lattice with k parameters $a_1, \ldots, a_k$. The dimension of $L^\times$ and $\bar{L}^\times$ is $n = n_1 + \cdots + n_k$, where n_i is the dimension of L_i.

Product lattices were first considered for quantization in [9]. It was shown in [15] that there exist optimal choices of the factors a_i in (6) that result in the lowest possible NSM of the product lattice. Such an *optimal product lattice* has an NSM satisfying

$$G(\bar{L}^\times)^n = G(L_1)^{n_1} \cdots G(L_k)^{n_k}. \tag{7}$$

By combining various lattices in this way and selecting the result with the lowest NSM for a given dimension n, many new lattices were found with lower NSMs than previously reported [15], [17].

A crucial result in [15] is that a product lattice (6) is never optimal. There always exists a small perturbation of the generator matrix of a product lattice that reduces the NSM, so that product lattices are not even locally optimal.

C. Glued lattices

The concept of "gluing" a lattice was originally developed by Conway and Sloane in [23] and later considered for quantization in [14]. It becomes especially useful when applied to product lattices, where it has led to two different 12-dimensional lattice quantizers with a lower NSM than the Coxeter–Todd lattice K_{12}.

[1] This notational assumption will, however, not prevent us from using nonsquare submatrices as building blocks in the square generator matrices (47) and (61).

Intuitively, gluing interpolates between a lattice L and its dual L^*,

$$L \subseteq L_{\text{gl}} \subseteq L^*, \tag{8}$$

where L_{gl} is the glued lattice. Since this requires that $L \subseteq L^*$, it implies that L must be an integral lattice. In general, the dual L^* of an integral lattice will not be an integral lattice unless L is self-dual.

Since an integral lattice L is contained in its dual L^*, the dual can be written as a finite number of unions of its translates

$$L^* = \bigcup_{\boldsymbol{g} \in L^*/L} (L + \boldsymbol{g}). \tag{9}$$

The quotient L^*/L is a largest set of vectors in L^* that are all distinct modulo translations by vectors in L. This set is not unique, but possible choices differ only by translations in L and therefore leave (9) invariant. Conventionally, the vectors are selected as short as possible within their coset $L + \boldsymbol{g}$, and by this convention, $\mathbf{0}$ is always one of the vectors. Thus, L^*/L is a finite set of coset representatives of L in L^* [1, p. 48]. The representatives $\boldsymbol{g}$ in (9) form a group under addition modulo L and are called the *glue vectors* of L. The number of glue vectors, i.e., the index of L in L^*, is $\det \boldsymbol{A}$.

We use the term "gluing" when a subset of glue vectors is used in (9),

$$L_{\text{gl}} \triangleq \bigcup_{\boldsymbol{g} \in \Gamma} (L + \boldsymbol{g}), \tag{10}$$

where $\Gamma \subseteq L^*/L$ is a group under addition modulo L, called the *glue group*. (If Γ is not a group, then (10) produces a nonlattice packing.)

A product lattice $L^\times$ with integral component lattices $L_1, \dots, L_k$, is itself an integral lattice and can thus be used for gluing. The glue vectors of $L^\times$ consist of concatenations of the glue vectors of L_i,

$$\boldsymbol{g} = [\boldsymbol{g}_1 \ \cdots \ \boldsymbol{g}_k], \tag{11}$$

where $\boldsymbol{g}_i \in L_i^*/L_i$, and are called *glue words*.

D. Gluing of scaled lattices

We generalize the gluing construction (10) by applying it to product lattices of the form (6) for arbitrary positive a_i, where the (unscaled) component lattices are integral lattices. For this, a useful identity that holds for any lattice L and scale factor $a > 0$ is that

$$(aL)^* = a^{-1} L^*, \tag{12}$$

which follows from the definition of the dual.

First, we define the gluing of scaled integral lattices. Let L be an integral lattice and Γ a glue group for L. By multiplying (10) on both sides with $a > 0$, we get

$$\bar{L}_{\text{gl}} \triangleq a L_{\text{gl}} = \bigcup_{\boldsymbol{g} \in \Gamma} (aL + a\boldsymbol{g}) = \bigcup_{\bar{\boldsymbol{g}} \in \bar{\Gamma}} (\bar{L} + \bar{\boldsymbol{g}}), \tag{13}$$

where we have defined $\bar{L} \triangleq aL$ and $\bar{\Gamma} \triangleq a\Gamma$. In general, $\bar{L} \not\subseteq \bar{L}^*$, so $\bar{L}_{\text{gl}}$ is not a glued lattice as defined in Sec. II-C since $\bar{L}^*/\bar{L}$ does not exist. However, by (12) we have $\bar{L}^* = (aL)^* = a^{-1} L^*$ and thus $\bar{L} = aL \subseteq aL^* = a^2 \bar{L}^*$. This means that there exist cosets

$$(a^2 \bar{L}^*)/\bar{L} = (aL^*)/(aL) = a\,(L^*/L) \tag{14}$$

(the factor a does not cancel since "/" forms the quotient space) and $\bar{\Gamma}$ is indeed a subset of coset representatives. We hence define the gluing of scaled integral lattices by (13).

For a product lattice $\bar{L}^\times$ of the form (6) with k integral component lattices $L_1, \dots, L_k$, we define gluing by composing glue words using the glue vectors of the scaled component lattices. Thus, let $\bar{\Gamma}^\times$ be a subgroup of

$$a_1\,(L_1^*/L_1) \times \cdots \times a_k\,(L_k^*/L_k), \tag{15}$$

which is a group under addition modulo $\bar{L}^\times$. Then, the glued scaled product lattice is

$$\bar{L}_{\text{gl}}^\times \triangleq \bigcup_{\bar{\boldsymbol{g}} \in \bar{\Gamma}^\times} (\bar{L}^\times + \bar{\boldsymbol{g}}). \tag{16}$$

Note that $\bar{L}_{\text{gl}}^\times$ is not necessarily a sublattice of the dual $(\bar{L}^\times)^*$ or of a scaled version of $(\bar{L}^\times)^*$.

E. Generalized gluing

The gluing constructions (10) and (16) can be generalized further as follows. We no longer require any relationship between the glue group and glue vectors of any constituent lattice. If L is an arbitrary lattice and Γ^{g} a finite group under addition modulo L, then

$$L_{\text{gl}}^{\text{g}} \triangleq \bigcup_{\boldsymbol{g} \in \Gamma^{\text{g}}} (L + \boldsymbol{g}) \tag{17}$$

still produces a lattice containing L. We call this "generalized gluing" to distinguish it from the classical gluing theory [23], [1, pp. 99–101]. This general case was mentioned in [14, Sec. III] but then not considered further. It contains the gluing of products of scaled integral lattices as a special case but also permits glue vectors not in L^* or non-integral L.

III. Parametric Voronoi Regions

We analyze lattices using the methods described in [16] with the optimizations in [24]. This is done by exactly constructing the full Voronoi region of the lattice up to symmetry. Using the recursion relations of [16, Sec. 3], which build upon [20, Sec. 3], the NSM (2) and second moment matrix (4) can then be calculated.

The Voronoi region of an n-dimensional lattice L is represented as a *hierarchy* of faces and subfaces, starting with the single n-dimensional face, the Voronoi region Ω, at the top with no parents (see, e.g., [16, Fig. 4]). The facets are the $(n-1)$-dimensional subfaces of Ω. Their only parent face is Ω. These facets are, like Ω, convex polytopes and each have $(n-2)$-dimensional subfaces (i.e., their respective facets), which are the $(n-2)$-faces of Ω. Our method builds the complete face hierarchy of Ω from the Voronoi region itself down to the 0-dimensional faces, which are the vertices of Ω. This hierarchy is sometimes called the *Hasse diagram.*

The automorphism group $\text{Aut}(L)$ of the lattice is a subgroup of the rotations $O(n)$ that takes L into L. If $\boldsymbol{B}$ is

a generator of L and $\boldsymbol{M} \in \mathrm{Aut}(L)$, then $\boldsymbol{BM}$ is another generator of the same lattice L. Symmetries are exploited in the following way. Since $\mathrm{Aut}(L)$ consists of the symmetries of Ω, it takes each d-dimensional face of Ω into another d-dimensional face of Ω. Two faces of Ω are called *equivalent* under $\mathrm{Aut}(L)$ if an element of $\mathrm{Aut}(L)$ takes one into the other. The hierarchy of faces we construct now only includes one face per class of equivalent faces, and additionally all their direct subfaces. (The latter are required to identify all classes of faces and to evaluate the recursion relations.)

Some issues are unique to analyzing a parametric lattice. Let $a_1, \dots, a_s$ be its s real parameters, $s \geq 1$, and $\boldsymbol{a} \triangleq [a_1, \dots, a_s]$. The generator matrix of a parametric lattice is then a function of the parameters, and we write it as $\boldsymbol{B}(\boldsymbol{a})$. Let further $\Omega(\boldsymbol{a})$ be the Voronoi region of the lattice generated by $\boldsymbol{B}(\boldsymbol{a})$. As the parameters approach certain critical points, vertices of $\Omega(\boldsymbol{a})$ may split into multiple vertices, or several vertices may merge into one or disappear. Such topological changes have to be considered when constructing a representation of the Voronoi region.

Our method builds the face hierarchy at a fixed point $\boldsymbol{a}$ in parameter space. We obtain the positions of all vertices, relevant vectors, and other quantities like the volumes of all faces and the NSM as functions of the parameters. However, since the face hierarchy is assumed fixed, these functions are valid only when $\Omega(\boldsymbol{a})$ undergoes no topological changes. If $\Omega(\boldsymbol{a})$ does undergo a topological change, our representation does not agree anymore with $\Omega(\boldsymbol{a})$ and may, in fact, become geometrically ill-defined.

To account for topological changes of the Voronoi region, we determine the region $P_{\boldsymbol{a}} \subset \mathbb{R}^s$ that contains $\boldsymbol{a}$ and where the Voronoi region has the same topology throughout. The region $P_{\boldsymbol{a}}$ is called the *phase* of $\boldsymbol{a}$. An example where phases of a parametric lattice have been analyzed can be found in [20, Sec. 4]. In particular, [20, Tab. 3] shows how the numbers of vertices and facets of the Voronoi region of the parametric lattice AE_9 change across phases.

The phase $P_{\boldsymbol{a}}$ is identified in two steps [16], [20]. First, we identify the region $P'_{\boldsymbol{a}}$, with $\boldsymbol{a} \in P'_{\boldsymbol{a}}$, where the lengths of all 1-faces are positive (recall that those lengths, i.e., the volumes of the 1-faces, are functions of $\boldsymbol{a}$). If the length of a 1-face vanishes, then two vertices merge and the face hierarchy must change. The second step is to test Ω for further topological changes in $P'_{\boldsymbol{a}}$ as described in the next paragraph. If no change occurs, then $P'_{\boldsymbol{a}} = P_{\boldsymbol{a}}$. Otherwise, the boundaries of $P_{\boldsymbol{a}}$ are located and the phase is determined as the interior region $P_{\boldsymbol{a}} \subset P'_{\boldsymbol{a}}$. For the lattices studied here, no such changes were found away from points of vanishing 1-face lengths, and thus for these lattices $P'_{\boldsymbol{a}} = P_{\boldsymbol{a}}$.

We use the following tests to identify topological changes of Ω within $P'_{\boldsymbol{a}}$. Each test is carried out at a large number of points (a few hundred for the lattices studied here) $\boldsymbol{a}' \in P'_{\boldsymbol{a}}$.[2]

(i) The set of parametric facets is the same throughout $P'_{\boldsymbol{a}}$. This is tested by writing the relevant vectors $\mathcal{N}(\boldsymbol{a})$ of $\Omega(\boldsymbol{a})$ as $\boldsymbol{uB}(\boldsymbol{a})$, for integer vectors $\boldsymbol{u}$, and checking that $\boldsymbol{uB}(\boldsymbol{a}')$ are the relevant vectors of $\Omega(\boldsymbol{a}')$ for the same set of integer vectors $\boldsymbol{u}$. This requires finding all relevant vectors once at each test point $\boldsymbol{a}'$ and writing them as linear combinations of the rows of $\boldsymbol{B}(\boldsymbol{a}')$.

(ii) Parametric vertices do not move outside of Ω. More precisely, let $\mathcal{V}_{\boldsymbol{a}}$ be the set of parametric vertices of $\Omega(\boldsymbol{a})$ and

$$\mathcal{V}_{\boldsymbol{a}}(\boldsymbol{a}') \triangleq \{\boldsymbol{v}(\boldsymbol{a}') \colon \boldsymbol{v}(\boldsymbol{a}) \in \mathcal{V}_{\boldsymbol{a}}\}\,. \tag{18}$$

Then we test if $\mathcal{V}_{\boldsymbol{a}}(\boldsymbol{a}') \subset \Omega(\boldsymbol{a}')$ as follows. The set of parametric vertices $\mathcal{V}_{\boldsymbol{a}}$ is constructed once at $\boldsymbol{a}$. Each vertex is then evaluated at $\boldsymbol{a}'$, which produces the set $\mathcal{V}_{\boldsymbol{a}}(\boldsymbol{a}')$. With the relevant vectors $\mathcal{N}(\boldsymbol{a}')$ known (see (i)), the set of inequalities that defines $\Omega(\boldsymbol{a}')$ is evaluated, i.e., we test

$$\boldsymbol{v} \cdot \boldsymbol{n} \leq \frac{1}{2}\|\boldsymbol{n}\|^2, \quad \forall \boldsymbol{v} \in \mathcal{V}_{\boldsymbol{a}}(\boldsymbol{a}'), \boldsymbol{n} \in \mathcal{N}(\boldsymbol{a}'). \tag{19}$$

(iii) Vertices do not move outside the facets they lie in; i.e., if a vertex $\boldsymbol{v}(\boldsymbol{a})$ lies in a facet $\mathcal{F}(\boldsymbol{a})$, then $\boldsymbol{v}(\boldsymbol{a}') \in \mathcal{F}(\boldsymbol{a}')$. This is tested as in ($ii$), but instead of checking for inequality in (19), it is verified that equality holds at $\boldsymbol{a}'$ if and only if it holds at $\boldsymbol{a}$. In practice, (ii) and (iii) are checked together.

(iv) The volume of the convex hull of $\mathcal{V}_{\boldsymbol{a}}(\boldsymbol{a}')$ is equal to $V(\boldsymbol{a}') = |\det \boldsymbol{B}(\boldsymbol{a}')|$. The volume of this convex hull is a byproduct of our calculations, making the test very inexpensive.

If condition (i) is not satisfied at $\boldsymbol{a}'$, then the set of faces has changed and our face hierarchy does not represent $\Omega(\boldsymbol{a}')$. Conditions (ii) and (iii) together ensure that $\mathcal{V}_{\boldsymbol{a}}(\boldsymbol{a}')$ are vertices of $\Omega(\boldsymbol{a}')$. The face hierarchy is then well-defined and represents a convex polytope Ω' contained in $\Omega(\boldsymbol{a}')$. Condition (iv) ensures that its volume agrees with the volume $V(\boldsymbol{a}')$ of $\Omega(\boldsymbol{a}')$, which then implies $\Omega' = \Omega(\boldsymbol{a}')$.

IV. Lattice Optimization

Numerical optimization of vector quantizers, i.e., finite sets of points, is a well-studied topic [25, Ch. 11], [7]. The complexity of such optimization algorithms increases exponentially with the dimension, if the number of bits available per dimension is fixed, and quickly gets out of hand. Therefore, algorithms to numerically optimize lattice quantizers were presented in [18], [21]. They work by iteratively updating the generator matrix towards lower NSMs, guided by stochastic gradient descent (SGD).[3] Thus, the algorithm has similarities with standard machine learning techniques, while remaining interpretable. It works without explicitly determining the Voronoi region, which is an extremely time- and memory-consuming operation in high dimensions.

[2] This works only if the number s of parameters is small. In cases of many parameters, testing the conditions on a dense enough set of points in $P'_{\boldsymbol{a}}$ might be too expensive.

[3] Recall from Sec. II-A that we use square generator matrices. With a nonsquare $n \times m$ generator, $m > n$, the SGD has a larger number of free parameters to optimize. However, since this lattice is equivalent to one with an $n \times n$ square generator, those extra degrees of freedom are redundant and cannot lead to new solutions. They merely rotate the lattice inside the higher-dimensional $\mathbb{R}^m$. We have not explored whether SGD with $m > n$ has better or worse convergence properties than SGD with $m = n$.

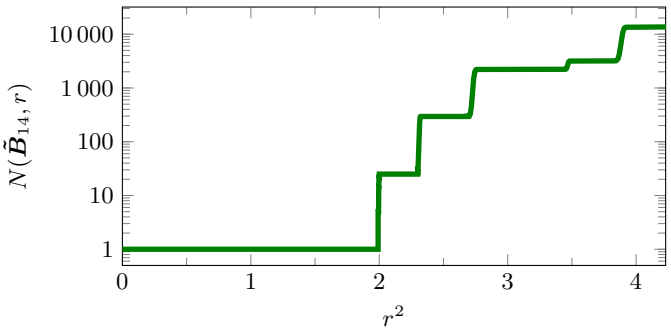

Fig. 1. Theta image of a numerically optimized 14-dimensional lattice. Note that N is constant almost everywhere and jumps discontinuously between integer values whenever r^2 passes the squared norm of a lattice point. The vertical steps are drawn as connected lines for visual purposes. The numerically optimized lattice shown here has well-separated spherical shells of many lattice points with almost equal norms, corresponding to large almost vertical steps.

The output of the numerical optimization algorithm is an approximation of a locally optimal lattice. Therefore, a heuristic method to identify the exact form of a lattice whose generator or Gram matrix is known only numerically was also proposed in [21]. It exploits the regular structure that almost all locally optimal lattices exhibit, specifically the arrangement of lattice points on a discrete set of separated, spherical shells.

To characterize, visualize, and identify these shells, the cumulative distribution of lattice point norms

$$N(\boldsymbol{B}, r) \triangleq |\{\boldsymbol{u} \in \mathbb{Z}^n \colon \|\boldsymbol{u}\boldsymbol{B}\| \leq r\}| \tag{20}$$

is used, where $\boldsymbol{B}$ is the generator matrix of the lattice. The plot of $N(\boldsymbol{B}, r)$ as a function of r^2 is called the *theta image* of $\boldsymbol{B}$ and an example for the 14-dimensional numerical result $\tilde{\boldsymbol{B}}_{14}$ (i.e., with approximate entries) of [21, Sec. VI] is shown in Fig. 1. Vertical steps in this plot, which represent the shells of lattice points with almost equal norms, are identified visually. They are turned into an overdetermined system of equations, which is then solved analytically using common mathematical software. The computational cost of this step depends on how many shells are used to construct the system of equations. In the cases studied here in 13 and 14 dimensions with 3 or fewer shells, solving the system had negligible cost. This procedure is described in detail in [21, Sec. V-B]. Three possible outcomes can occur now: the system has one, multiple, or no solution. If it has one solution, then the exact lattice is recovered. The case of multiple solutions corresponds to a parametric lattice. In the rare cases when the target lattice does not have a structure of well-separated shells, the identification technique fails. The first such case we have observed appears in 13 dimensions and will be described in detail in Sec. VI.

In the remainder of this section, we introduce a deterministic algorithm to fine-tune and exactly identify a locally optimal lattice from a closesecond approximation, without relying on any presumed lattice structure. It is very demanding in terms of computer time and memory, and we apply it only as a last resort when the identification method in [21] fails to return an exact, locally optimal lattice.

A second moment matrix $\boldsymbol{U}$ that is not proportional to the identity can be used to find a deformation $\boldsymbol{A}_\epsilon$ of any lattice L with generator $\boldsymbol{B}$ towards a lower NSM. This idea is introduced in the proof of [15, Theorem 2]. Let

$$\bar{\boldsymbol{U}} \triangleq \boldsymbol{U} - \frac{\operatorname{tr}\boldsymbol{U}}{n}\boldsymbol{I}_n \tag{21}$$

be the traceless part of $\boldsymbol{U}$, which is nonzero if $\boldsymbol{U}$ is not proportional to $\boldsymbol{I}_n$, and $\boldsymbol{A}_\epsilon \triangleq \exp(-\epsilon\bar{\boldsymbol{U}})$. It is then shown in [15] that for small enough positive ϵ, the lattice $L\boldsymbol{A}_\epsilon$ with generator $\boldsymbol{B}\boldsymbol{A}_\epsilon$ has a lower NSM than L.

An optimization algorithm based on this insight operates as follows. Starting from an arbitrary lattice L with generator matrix $\boldsymbol{B}$, the full face hierarchy of the Voronoi region, from dimension 0 to n, is computed. From this description, the NSM G and the second moment matrix $\boldsymbol{U}$ are computed exactly. A perturbation matrix $\boldsymbol{A}_\epsilon = \exp(-\epsilon\bar{\boldsymbol{U}})$ is computed with $\bar{\boldsymbol{U}}$ given by (21). An alternative is $\boldsymbol{A}_\epsilon = \boldsymbol{I}_n - \epsilon\bar{\boldsymbol{U}}$, which is approximately equivalent to $\exp(-\epsilon\bar{\boldsymbol{U}})$ if the elements of $\epsilon\bar{\boldsymbol{U}}$ have small enough magnitude. Then the generator matrix $\boldsymbol{B}$ is perturbed into $\boldsymbol{B}\boldsymbol{A}_\epsilon$. This yields a parametric lattice $L\boldsymbol{A}_\epsilon$, with ϵ as a parameter.

To select ϵ, we consider the deformed Voronoi region $\Omega\boldsymbol{A}_\epsilon$, where Ω is the Voronoi region of L. This region is different from the Voronoi region of $L\boldsymbol{A}_\epsilon$, but it is easy to compute from Ω when $\boldsymbol{A}_\epsilon$ is known. The second moment matrix of $\Omega\boldsymbol{A}_\epsilon$ is $\boldsymbol{A}_\epsilon^T\boldsymbol{U}\boldsymbol{A}_\epsilon$ [15, Theorem 2]. In general, there exists no perturbation ϵ that makes $\boldsymbol{A}_\epsilon^T\boldsymbol{U}\boldsymbol{A}_\epsilon$ proportional to $\boldsymbol{I}_n$, but ϵ can nevertheless be chosen to move the off-diagonal elements closer to zero and the diagonal elements closer to each other. This provides a good enough approximation for the next step.

At this point it may be useful to introduce additional parameters into the parametric lattice. This is not strictly necessary but can significantly reduce the number of steps needed for the optimization algorithm to converge. It is motivated by the fact that there may be no value of ϵ for which $L\boldsymbol{A}_\epsilon$ has a second moment matrix proportional to $\boldsymbol{I}_n$. An example is the 13-dimensional case studied in Sec. VI, which is a generalized glued product of three integral lattices. There, a natural choice of additional parameters are the scale factors $\boldsymbol{a} = [a_1, a_2, a_3]$ of the component lattices.

Next, the face hierarchy of $L\boldsymbol{A}_\epsilon$ is computed for the selected ϵ. This yields a complete description of the Voronoi region at ϵ and within the phase $P_{\epsilon,\boldsymbol{a}}$. This is why the exact value of ϵ is not critical. The NSM is computed as a function of ϵ and any additional parameters in the phase and the minimum is found analytically. If this minimum lies in $P_{\epsilon,\boldsymbol{a}}$, then the algorithm has converged; otherwise the search continues in another phase. There are at least three methods to select the next phase to investigate.

One is to consider the phase in which the minimum of the NSM expression of $P_{\epsilon,\boldsymbol{a}}$ lies. Although this expression does not give the NSM in other phases, it is often a very accurate approximation. For example, (66) shows that the normalized second moment of the 13-dimensional parametric lattice in Sec. VI is 13 times differentiable on the boundary between the two analyzed phases.

The second method is to compute the second moment matrix of $L\boldsymbol{A}_\epsilon$ and again perturb the lattice to move this matrix closer to a scaled identity. With this and the previous method, it needs to be verified that the exact NSM at the new point is less than the previous NSM.

If this is not the case (which is theoretically possible although we have not experienced it in practice), then a third, safer, method is to numerically find the minimum NSM in $P_{\epsilon,\boldsymbol{a}}$, which by assumption lies on the phase boundary, and next investigate the other phases that touch the boundary at the same point, proceeding with the ones containing the smallest NSM.

We successfully used the first of these three options to optimize the 13-dimensional lattice studied here. This required computing the face hierarchy at the initial point and in two additional phases. The 14-dimensional lattice was optimized in just a single step, since its second moment matrix was proportional to $\boldsymbol{I}_n$ within the initial phase.

V. Dimension 14: Glued $K_{10}' \times D_4$

The new lattices studied in this paper were initially found numerically in [21]. In dimensions 10–16, the gradient descent method numerically minimized the NSM, starting from random lattices. After 100 such searches were performed in each dimension, the lattice with the lowest NSM was selected for further analysis. In all of these dimensions except 13 and 14, the system of equations obtained from the theta image has a unique solution and the resulting lattices can thus be represented by an exact generator matrix $\boldsymbol{B}$.

This section analyzes the previously unidentified lattice in dimension 14. We start with the 14-dimensional lattice as its analysis is less complicated and establishes the basic steps upon which the analysis of the 13-dimensional lattice then builds.

A. Identification of the lattice

The system of equations built from the theta image of the numerically found 14-dimensional lattice in Fig. 1 is underdetermined, regardless of how many shells are considered. Although the Gram matrix cannot be uniquely determined at this stage, it contains only one unknown, real parameter. Thus, the new 14-dimensional lattice is a parametric lattice with one degree of freedom.

A generator matrix was obtained from the Gram matrix by Cholesky decomposition, and the generator matrix was further refined via basis changes, rotations, and scaling, aiming to confine the influence of the real parameter cleanly to as few dimensions as possible. This process is the only one in going from an approximate to an exact generator matrix that we can presently not automate or give an algorithm for. It requires intuition to find suitable transformations that subsequently allow the identification of the geometrical structure, e.g., as a glued product of known lattices.

For the 14-dimensional case, the parametric generator matrix

$$\boldsymbol{B}_{14}(a) = \left[\begin{array}{cccccccccc:cccc}
2 & 0 & 0 & 0 & 0 & 0 & 0 & 0 & 0 & 0 & 0 & 0 & 0 & 0 \\
1 & q & 0 & 0 & 0 & 0 & 0 & 0 & 0 & 0 & 0 & 0 & 0 & 0 \\
0 & 0 & 2 & 0 & 0 & 0 & 0 & 0 & 0 & 0 & 0 & 0 & 0 & 0 \\
0 & 0 & 1 & q & 0 & 0 & 0 & 0 & 0 & 0 & 0 & 0 & 0 & 0 \\
0 & 0 & 0 & 0 & 2 & 0 & 0 & 0 & 0 & 0 & 0 & 0 & 0 & 0 \\
0 & 0 & 0 & 0 & 1 & q & 0 & 0 & 0 & 0 & 0 & 0 & 0 & 0 \\
1 & 0 & \frac{1}{2} & -\frac{q}{2} & \frac{1}{2} & -\frac{q}{2} & 1 & 0 & 0 & 0 & 0 & 0 & 0 & 0 \\
\frac{1}{2} & \frac{q}{2} & 1 & 0 & 1 & 0 & \frac{1}{2} & \frac{q}{2} & 0 & 0 & 0 & 0 & 0 & 0 \\
\frac{1}{2} & -\frac{q}{2} & 1 & 0 & \frac{1}{2} & -\frac{q}{2} & 0 & 0 & 1 & 0 & 0 & 0 & 0 & 0 \\
1 & 0 & \frac{1}{2} & \frac{q}{2} & 1 & 0 & 0 & 0 & \frac{1}{2} & \frac{q}{2} & 0 & 0 & 0 & 0 \\
\hdashline
1 & 0 & 1 & 0 & \frac{1}{2} & \frac{q}{2} & 0 & 0 & 0 & 0 & a & 0 & 0 & 0 \\
0 & 0 & 0 & 0 & 0 & 0 & 0 & 0 & 0 & 0 & -a & a & 0 & 0 \\
0 & 0 & 0 & 0 & 0 & 0 & 0 & 0 & 0 & 0 & -a & 0 & a & 0 \\
\frac{1}{2} & -\frac{q}{2} & \frac{1}{2} & -\frac{q}{2} & 1 & 0 & 0 & 0 & 0 & 0 & \frac{a}{2} & \frac{a}{2} & \frac{a}{2} & \frac{a}{2}
\end{array}\right] \tag{22}$$

was obtained, where $q \triangleq \sqrt{3}$ and a is the unknown parameter. The lattice generated by (22) may be obtained by gluing scaled integral lattices. We set $k = 2$, $L_1 = K_{10}'$, $L_2 = D_4$, $a_1 = 1$, and $a_2 = a$ in (6) and (16) to obtain

$$L_{14} \triangleq \bar{L}_{\text{gl}}^{\times} = \bigcup_{[\boldsymbol{g}_1\ \boldsymbol{g}_2] \in \bar{\Gamma}^{\times}} (K_{10}' + \boldsymbol{g}_1) \times (aD_4 + \boldsymbol{g}_2). \tag{23}$$

Here, K_{10}' is a laminated 10-dimensional lattice [26, Sec. 8.5], which is equivalent to the lattice with automorphism group $(C_6 \times \mathrm{SU}_4(2)) \colon C_2$ described in [27],[4] and D_4 is the 4-dimensional checkerboard lattice. We can for example take the top-left 10×10 submatrix of (22) as a generator matrix for K_{10}' and [18, Eq. (36)] as a generator matrix for D_4. With these choices, the glue group $\bar{\Gamma}^{\times}$ may be represented by the four vectors

$$\begin{array}{l}
\left[\begin{array}{cccccccccccccc} 0 & 0 & 0 & 0 & 0 & 0 & 0 & 0 & 0 & 0 & 0 & 0 & 0 & 0 \end{array}\right], \\
\left[\begin{array}{cccccccccccccc} 1 & 0 & 1 & 0 & \frac{1}{2} & \frac{q}{2} & 0 & 0 & 0 & 0 & a & 0 & 0 & 0 \end{array}\right], \\
\left[\begin{array}{cccccccccccccc} \frac{1}{2} & -\frac{q}{2} & \frac{1}{2} & -\frac{q}{2} & 1 & 0 & 0 & 0 & 0 & 0 & \frac{a}{2} & \frac{a}{2} & \frac{a}{2} & \frac{a}{2} \end{array}\right], \\
\left[\begin{array}{cccccccccccccc} \frac{1}{2} & \frac{q}{2} & \frac{1}{2} & \frac{q}{2} & -\frac{1}{2} & \frac{q}{2} & 0 & 0 & 0 & 0 & \frac{a}{2} & -\frac{a}{2} & -\frac{a}{2} & -\frac{a}{2} \end{array}\right].
\end{array} \tag{24}$$

The first 10 components of each vector in (24) form a subgroup of L_1^*/L_1, and the last 4 components of the same vectors form the whole group $a\,(L_2^*/L_2)$. For $a = 1$, the 14-dimensional vectors (24) therefore form a subgroup of $(L^{\times})^*/L^{\times}$ for the product lattice $L^{\times} = L_1 \times L_2$. Together, (23) and (24) define the same lattice as (22).

B. Construction of the Voronoi region

Even though the parameter a cannot be determined exactly from the system of equations obtained from the theta image, it can still be identified approximately. The theta image of $\boldsymbol{B}_{14}(a)$, properly scaled, best matches Fig. 1 for $a \approx 25/19$.

[4] Their equivalence is proved in Appendix B-A.

The Voronoi region of the lattice (22) was constructed at $a = 25/19 \approx 1.3158$ as described in Sec. III. The phase P_a is given by

$$\sqrt{5/3} < a < \sqrt{13/7}, \tag{25}$$

i.e., $1.291 \lesssim a \lesssim 1.363$. Conditions (i)–(iv) of Sec. III are fulfilled in this interval, but not outside. At both of these boundaries, at least one class of 1-faces has zero length: the two vertices at their endpoints merge to one.

The automorphism group $\mathrm{Aut}(L_{14})$ of the lattice (22) has order 59 719 680. It is a subgroup of the direct product $O(10)\times O(4)$, i.e., all symmetries $\boldsymbol{M} \in \mathrm{Aut}(L_{14})$ are of the form

$$\boldsymbol{M} = \begin{bmatrix} \boldsymbol{M}_{10\times 10} & \boldsymbol{0} \\ \boldsymbol{0} & \boldsymbol{M}_{4\times 4} \end{bmatrix}, \tag{26}$$

where $\boldsymbol{M}_{d\times d}$ is an orthogonal $d \times d$ matrix. Let $\pi_{10}\colon \mathrm{Aut}(L_{14}) \to O(10)$ and $\pi_4\colon \mathrm{Aut}(L_{14}) \to O(4)$ be the projections that map a symmetry $\boldsymbol{M} \in \mathrm{Aut}(L_{14})$ of the form (26) to its corresponding 10×10 and 4×4 blocks $\boldsymbol{M}_{10\times 10}$ and $\boldsymbol{M}_{4\times 4}$, respectively. Then, $\pi_{10}(\mathrm{Aut}(L_{14}))$ is a group of order 311 040 that is the symmetry group of K'_{10}, whose order has been reported in [28, lattice *KAPPA10′*]. Similarly, $\pi_4(\mathrm{Aut}(L_{14}))$ is a group of order 1 152 that is the automorphism group of D_4 [1, Ch. 4]. However, while the product

$$\pi_{10}(\mathrm{Aut}(L_{14})) \times \pi_4(\mathrm{Aut}(L_{14})) \tag{27}$$

of these two groups (which has order 358 318 080) is the automorphism group of the (unglued) product lattice $K'_{10} \times aD_4$, it is *not* the automorphism group of the glued lattice (22).

The subgroup

$$\mathcal{G}_{10} \triangleq \pi_4^{-1}(\boldsymbol{I}_4) = \{\boldsymbol{M} \in \mathrm{Aut}(L_{14})\colon \pi_4(\boldsymbol{M}) = \boldsymbol{I}_4\}, \tag{28}$$

which affects only the first 10 components, has order 51 840. Therefore, $\mathcal{G}_{10}$ is isomorphic to a *strict* subgroup of $\pi_{10}(\mathrm{Aut}(L_{14}))$. For the following discussion, it is helpful to define the embeddings

$$\begin{aligned} i_{10}(\boldsymbol{M}_{10\times 10}) &\triangleq \begin{bmatrix} \boldsymbol{M}_{10\times 10} & \boldsymbol{0} \\ \boldsymbol{0} & \boldsymbol{I}_4 \end{bmatrix}, \\ i_4(\boldsymbol{M}_{4\times 4}) &\triangleq \begin{bmatrix} \boldsymbol{I}_{10} & \boldsymbol{0} \\ \boldsymbol{0} & \boldsymbol{M}_{4\times 4} \end{bmatrix}. \end{aligned} \tag{29}$$

The group $\mathcal{G}_{10}$ is then generated by the following eight matrices:

- five matrices $\boldsymbol{M}^{(1)}, \ldots, \boldsymbol{M}^{(5)}$ producing sign-changes of component pairs (x_{2i-1}, x_{2i}), where x_j is the jth component of a lattice vector $\boldsymbol{x}$ and $i = 1, \ldots, 5$,
- one matrix $\boldsymbol{M}^{(6)}$ for the joint swapping of pairs (x_1, x_2) with (x_3, x_4) and (x_7, x_8) with (x_9, x_{10}),
- one matrix $\boldsymbol{M}^{(7)}$ for the joint swapping of pairs (x_3, x_4) with (x_7, x_8) and (x_5, x_6) with (x_9, x_{10}),
- one matrix $\boldsymbol{M}^{(8)} \triangleq i_{10}(\boldsymbol{M}^{(8)}_{10})$, where

$$\boldsymbol{M}^{(8)}_{10} \triangleq \begin{bmatrix} \boldsymbol{I}_2/2 & \boldsymbol{W} & \boldsymbol{W} & -\boldsymbol{I}_2/2 & \boldsymbol{0} \\ \boldsymbol{W}^T & \boldsymbol{I}_2/2 & -\boldsymbol{I}_2/2 & \boldsymbol{W}^T & \boldsymbol{0} \\ \boldsymbol{W}^T & -\boldsymbol{I}_2/2 & \boldsymbol{I}_2/2 & \boldsymbol{W}^T & \boldsymbol{0} \\ -\boldsymbol{I}_2/2 & \boldsymbol{W} & \boldsymbol{W} & \boldsymbol{I}_2/2 & \boldsymbol{0} \\ \boldsymbol{0} & \boldsymbol{0} & \boldsymbol{0} & \boldsymbol{0} & \boldsymbol{I}_2 \end{bmatrix} \tag{30}$$

with

$$\boldsymbol{W} \triangleq \frac{1}{4}\begin{bmatrix} 1 & -\sqrt{3} \\ \sqrt{3} & 1 \end{bmatrix}. \tag{31}$$

The eight group generators $\boldsymbol{M}^{(1)}, \ldots, \boldsymbol{M}^{(8)}$ each have order 2, but they do not correspond to the prime powers in $51\,840 = 2^7 3^4 5$. In fact, the group generated by $\{\boldsymbol{M}^{(6)}, \boldsymbol{M}^{(7)}\}$ has order 10 and together with $\boldsymbol{M}^{(1)}, \ldots, \boldsymbol{M}^{(5)}$ generates a group of order $320 = 2^5 \cdot 10$. Adding $\boldsymbol{M}^{(8)}$ to the set of generators increases the group order to 51 840. We found no simple product decomposition allowing $\mathcal{G}_{10}$ to be expressed as product of subgroups whose orders correspond to prime powers.

The symmetries of the automorphism group of K'_{10} that are missing from $\mathcal{G}_{10}$ are generated by

$$\boldsymbol{M}_{10} = \begin{bmatrix} \boldsymbol{M}_2 & \boldsymbol{0} & \boldsymbol{0} & \boldsymbol{0} & \boldsymbol{0} \\ \boldsymbol{0} & \boldsymbol{0} & \boldsymbol{M}''_2 & \boldsymbol{0} & \boldsymbol{0} \\ \boldsymbol{0} & \boldsymbol{M}''_2 & \boldsymbol{0} & \boldsymbol{0} & \boldsymbol{0} \\ \boldsymbol{0} & \boldsymbol{0} & \boldsymbol{0} & \boldsymbol{M}_2 & \boldsymbol{0} \\ \boldsymbol{0} & \boldsymbol{0} & \boldsymbol{0} & \boldsymbol{0} & \boldsymbol{M}'_2 \end{bmatrix} \tag{32}$$

and

$$\boldsymbol{M}'_{10} = \begin{bmatrix} \boldsymbol{M}_2 & \boldsymbol{0} & \boldsymbol{0} & \boldsymbol{0} & \boldsymbol{0} \\ \boldsymbol{0} & \boldsymbol{0} & \boldsymbol{0} & \boldsymbol{0} & \boldsymbol{M}_2 \\ \boldsymbol{0} & \boldsymbol{M}_2 & \boldsymbol{0} & \boldsymbol{0} & \boldsymbol{0} \\ \boldsymbol{0} & \boldsymbol{0} & \boldsymbol{M}_2 & \boldsymbol{0} & \boldsymbol{0} \\ \boldsymbol{0} & \boldsymbol{0} & \boldsymbol{0} & \boldsymbol{M}_2 & \boldsymbol{0} \end{bmatrix}, \tag{33}$$

where

$$\begin{gathered} \boldsymbol{M}_2 \triangleq \frac{1}{2}\begin{bmatrix} 1 & -\sqrt{3} \\ -\sqrt{3} & -1 \end{bmatrix}, \qquad \boldsymbol{M}'_2 \triangleq \frac{1}{2}\begin{bmatrix} 1 & \sqrt{3} \\ \sqrt{3} & -1 \end{bmatrix}, \\ \boldsymbol{M}''_2 \triangleq \mathrm{diag}(1, -1). \end{gathered} \tag{34}$$

Note that $i_{10}(\boldsymbol{M}_{10})$ and $i_{10}(\boldsymbol{M}'_{10})$ are *not* symmetries of the glued lattice (22).

We can also describe the subgroup $\mathcal{G}_4 \triangleq \pi_{10}^{-1}(\boldsymbol{I}_{10}) \subset \mathrm{Aut}(L_{14})$ of symmetries affecting only the last 4 components. It consists of all permutations and an even number of sign changes of the last four components. Together, these form a group of order 192 that is isomorphic to a subgroup of the automorphism group of D_4. The remaining symmetries of D_4

are, however, not found in $\mathcal{G}_4$. They consist of the Hadamard matrix

$$\boldsymbol{M}_4 \triangleq \frac{1}{2}\begin{bmatrix} 1 & 1 & 1 & 1 \\ 1 & -1 & 1 & -1 \\ 1 & 1 & -1 & -1 \\ 1 & -1 & -1 & 1 \end{bmatrix} \tag{35}$$

and a sign change of the last component,

$$\boldsymbol{M}'_4 \triangleq \operatorname{diag}(1, 1, 1, -1). \tag{36}$$

The subgroups $\mathcal{G}_{10}$ and $\mathcal{G}_4$ together form a group of order 9 953 280. By combining the generators of $\mathcal{G}_{10}$ with those of $\mathcal{G}_4$ and the two matrices

$$\begin{bmatrix} \boldsymbol{M}_{10} & \boldsymbol{0} \\ \boldsymbol{0} & \boldsymbol{M}_4 \end{bmatrix} \quad \text{and} \quad \begin{bmatrix} \boldsymbol{M}'_{10} & \boldsymbol{0} \\ \boldsymbol{0} & \boldsymbol{M}'_4 \end{bmatrix}, \tag{37}$$

we finally obtain the full group $\operatorname{Aut}(L_{14})$.

In practice, we found this group by first forming the direct product of the known automorphism groups of K'_{10} and D_4. As noted above, $\operatorname{Aut}(L_{14})$ is a strict subgroup of this larger group. We then used GAP [29] to initially determine $\mathcal{G}_{10}$ and $\mathcal{G}_4$ and subsequently analyzed combinations of the symmetries of K'_{10} and D_4 missing from $\mathcal{G}_{10}$ and $\mathcal{G}_4$.

C. Optimization of the NSM

The NSM as a function of a, $G(a)$, is given by (2) with $n = 14$, $V(a) = |\det \boldsymbol{B}_{14}(a)| = 9\sqrt{3}a^4$, and

$$\begin{aligned}\int_\Omega \|\boldsymbol{x}\|^2 \,\mathrm{d}\boldsymbol{x} = \frac{\sqrt{3}}{2^{24}\cdot 3^{13}\cdot 5^6\cdot 7^4\cdot 11^2\cdot 13 a^4}\\ \big(-2036206247431384 87a^{30}\\ +3801139170184845180a^{28}\\ -1238953978448290723 5a^{26}\\ -3606900993863642966 40a^{24}\\ +6016931591463402618645a^{22}\\ -5032877267998388773 3644a^{20}\\ +2811881640166930163 48265a^{18}\\ -1139254272224209154 665080a^{16}\\ +3445025447618975371 649355a^{14}\\ -7776389251376810821 296540a^{12}\\ +1582506837252495638 4278439a^{10}\\ +6097536730919383009 631280a^8\\ +6105246565601165070 721815a^6\\ -2678596597802952982 813140a^4\\ +7036358221300795401 68595a^2\\ -8399480329602983494 3608\big).\end{aligned} \tag{38}$$

Fig. 2 shows a plot of $G(a)$ in the phase (25). It has its minimum at the only root of $G'(a)$ in this phase. We define

$$f(a^2) \triangleq 3^{-\frac{9}{14}} a^{\frac{67}{7}} G'(a) \tag{39}$$

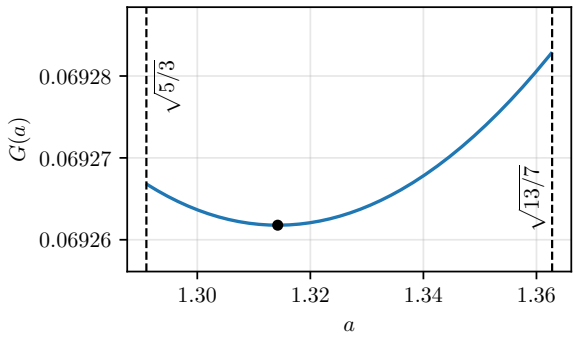

Fig. 2. NSM for the 14-dimensional lattice (22) as function of a. The dot marks the location of the minimum and the dashed vertical lines indicate the boundaries of the phase (25). The previously reported minimum NSM of 0.069 52 [17] is about eight plot-heights above the dot.

and $v \triangleq a^2$ to obtain a polynomial of degree 15 with rational coefficients, namely

$$\begin{aligned} f(v) = \frac{1}{2^{24}\cdot 3^{15}\cdot 5^5\cdot 7^6\cdot 11^2\cdot 13}\\ \big(-1018103123715692435v^{15}\\ +1723183090483796481 6v^{14}\\ -5038412845689715608 9v^{13}\\ -1298484357790911467904v^{12}\\ +1885305231991866153842 1v^{11}\\ -1342100604799570339563 84v^{10}\\ +6186139608367246359661 83v^9\\ -1974707405188629201419472v^8\\ +4363698900317368804089183v^7\\ -6221111401101448657037232v^6\\ +5275022790841652128092813v^5\\ -8130048974559177346175 04v^4\\ -3663147939360699042433089v^3\\ +2857169704323149848334016v^2\\ -1078908260599455294925179v\\ +1679896065920596698872 16\big). \end{aligned} \tag{40}$$

If v_0 denotes the second positive root of f, then the minimum of $G(a)$ lies at

$$a_{\text{opt}} = \sqrt{v_0} \approx 1.314\,224\,989\,311, \tag{41}$$

leading to an NSM of

$$G(a_{\text{opt}}) \approx 0.069\,261\,778\,717. \tag{42}$$

We will refer to the lattice generated by $\boldsymbol{B}_{14}(a_{\text{opt}})$ as $\mathrm{K'D}_{14}^{\mathrm{gl}}$. The numerically estimated NSM was $0.069\,261 \pm 0.000\,002$ [21, Tab. II].

For comparison, the previously lowest reported NSM in 14 dimensions is 0.069 52 [17], which is higher than the NSM of (22) for any a in the phase (25).

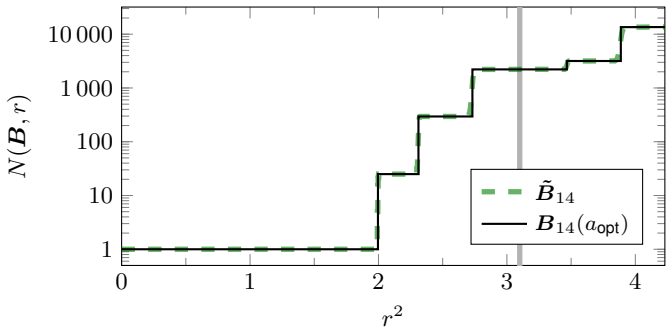

Fig. 3. Theta image of the conjectured optimal 14-dimensional lattice, rescaled to determinant 1 and superimposed on the theta image of the numerically optimized lattice in Fig. 1. The three shells to the left of the gray bar were used to determine the parametric lattice from the numerical one.

We also calculated the second moment matrix (4) of the lattice (22) as a function of a. It is

$$\boldsymbol{U} = \begin{bmatrix} \alpha(a)\boldsymbol{I}_{10} & \boldsymbol{0} \\ \boldsymbol{0} & \beta(a)\boldsymbol{I}_4 \end{bmatrix}, \tag{43}$$

where

$$\begin{aligned} \alpha(a) &= V(a)^{\frac{1}{7}} G(a) - \frac{5103}{10V(a)^2} f(a^2) \\ \beta(a) &= V(a)^{\frac{1}{7}} G(a) + \frac{5103}{4V(a)^2} f(a^2). \end{aligned} \tag{44}$$

Recall that a necessary (but not sufficient) condition for the optimality of a lattice quantizer is that $\boldsymbol{U}$ is proportional to the identity matrix. From (44), it is clear that $\boldsymbol{U} \propto \boldsymbol{I}_{14}$ is equivalent to $f(a^2) = 0$ and thus also equivalent to $G'(a) = 0$. This condition is satisfied at a_{opt}. Although this is only a necessary condition for local optimality, we conjecture that $\mathrm{K'D}_{14}^{\text{gl}}$, which is generated by $\boldsymbol{B}_{14}(a_{\text{opt}})$, is not only the locally optimal but also the globally optimal 14-dimensional lattice quantizer. The exact theta image of the new lattice is shown in Fig. 3.

D. Further properties of the Voronoi region

The Voronoi region of the lattice (22) in phase (25) has 13 542 facets, 1 669 150 800 vertices, and overall 5 223 614 689 453 faces in dimensions 0 through 14. Under its automorphism group the individual number of classes of faces in dimensions 0 through 14 is, respectively, 747, 6 211, 24 871, 60 135, 94 264, 100 782, 76 698, 42 880, 17 739, 5 345, 1 166, 195, 31, 5, and 1, making in total 431 070 equivalence classes of faces across all dimensions.

The lattice has 24 shortest nonzero vectors, which is its *kissing number*. The lengths of these determine the *packing radius* and *packing density*, respectively

$$\begin{aligned} \rho &= \frac{a}{\sqrt{2}}, \\ \Delta &\triangleq \frac{V_{14}\rho^{14}}{|\det \boldsymbol{B}_{14}(a)|} = \frac{\pi^7 a^{10}}{5\,806\,080\,\sqrt{3}}, \end{aligned} \tag{45}$$

where V_{14} is the volume of the 14-dimensional unit ball. At a_{opt}, the corresponding numerical values are approximately $\rho \approx 0.929\,297$ and $\Delta \approx 0.004\,616$.

The *covering radius* and *covering thickness*, which are respectively

$$\begin{aligned} R &= \sqrt{\frac{(a^2+3)(3a^2+1)}{6a^2}}, \\ \Theta &\triangleq \frac{V_{14}R^{14}}{|\det \boldsymbol{B}_{14}(a)|} = \frac{\sqrt{3}\pi^7(a^2+3)^7(3a^2+1)^7}{38\,093\,690\,880\,a^{18}}, \end{aligned} \tag{46}$$

are determined by the circumradius of the Voronoi region: the maximum distance of its vertices from the origin. At a_{opt}, these are respectively approximately $R \approx 1.679\,211$ and $\Theta \approx 18.264\,550$.

For comparison, in dimension 14 the highest known lattice packing density is $\Delta(\Lambda_{14}) \approx 0.021\,624$ [1, Tab. 1.2] and the lowest known lattice covering thickness is $\Theta(\mathsf{L}_{14}^c) \approx 8.825\,210$ [30, Tab. 2]. These values show that a good lattice quantizer is not necessarily good for packing or covering or has a high kissing number. A similar phenomenon had been observed already in 1998 by Agrell and Eriksson (see the second paragraph following [18, Eq. (31)]), where the conjectured optimal lattice quantizer in 9 dimensions, AE_9, was described with a kissing number of only 2.

VI. Dimension 13: Glued $A_7 \times D_5 \times \mathbb{Z}$

A. Identification based on the theta image

The theta image of the numerical lattice with the lowest NSM we found in 13 dimensions is shown in Fig. 4. When compared with the 14-dimensional lattice in Fig. 1, the vertical steps are not as clearly separated from each other. Nevertheless, the same identification technique [21] was applied and yielded in this case an exact lattice L'_{13}, with no unknown parameter. We identified L'_{13} as glued $A_7 \times D_5 \times \sqrt{2}\mathbb{Z}$, with generator

$$\boldsymbol{B}'_{13} = \left[\begin{array}{cccccccc:ccccc} -1 & 1 & 0 & 0 & 0 & 0 & 0 & 0 & 0 & 0 & 0 & 0 & 0 \\ -1 & 0 & 1 & 0 & 0 & 0 & 0 & 0 & 0 & 0 & 0 & 0 & 0 \\ -1 & 0 & 0 & 1 & 0 & 0 & 0 & 0 & 0 & 0 & 0 & 0 & 0 \\ -1 & 0 & 0 & 0 & 1 & 0 & 0 & 0 & 0 & 0 & 0 & 0 & 0 \\ -1 & 0 & 0 & 0 & 0 & 1 & 0 & 0 & 0 & 0 & 0 & 0 & 0 \\ -1 & 0 & 0 & 0 & 0 & 0 & 1 & 0 & 0 & 0 & 0 & 0 & 0 \\ -1 & 0 & 0 & 0 & 0 & 0 & 0 & 1 & 0 & 0 & 0 & 0 & 0 \\ \hdashline 0 & 0 & 0 & 0 & 0 & 0 & 0 & 0 & 2 & 0 & 0 & 0 & 0 \\ 0 & 0 & 0 & 0 & 0 & 0 & 0 & 0 & 1 & 1 & 0 & 0 & 0 \\ 0 & 0 & 0 & 0 & 0 & 0 & 0 & 0 & 1 & 0 & 1 & 0 & 0 \\ 0 & 0 & 0 & 0 & 0 & 0 & 0 & 0 & 1 & 0 & 0 & 1 & 0 \\ 0 & 0 & 0 & 0 & 0 & 0 & 0 & 0 & 1 & 0 & 0 & 0 & 1 \\ \hdashline \frac{11}{16} & \frac{11}{16} & \frac{11}{16} & -\frac{5}{16} & -\frac{5}{16} & -\frac{5}{16} & -\frac{5}{16} & -\frac{5}{16} & \frac{1}{2} & \frac{1}{2} & \frac{1}{2} & \frac{1}{2} & \frac{1}{2} \end{array}\right]. \tag{47}$$

This is a case of generalized gluing as described in Sec. II-E. The scale factor $\sqrt{2}$ serves to give all three component lattices the same shortest vector norm $\sqrt{2}$. We defer a description of the gluing structure to the more generic lattice (61), of which $\boldsymbol{B}'_{13}$ is a special case.

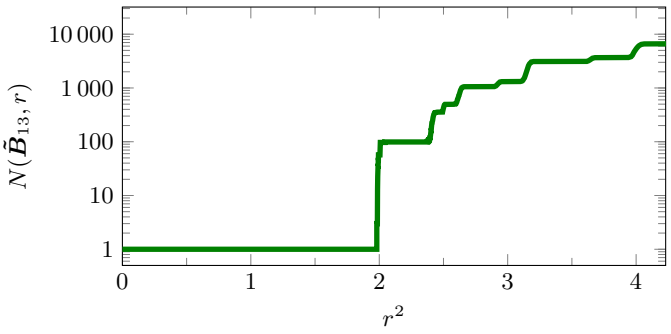

Fig. 4. Theta image of a numerically optimized 13-dimensional lattice.

The lattice L'_{13} was analyzed using the methods in [16], [24]. This was easier than for the 14-dimensional lattice because there is no free parameter. The resulting NSM

$$G = \frac{26464302520815850291209820565874314628 7}{2^{81} \cdot 3^9 \cdot 5^3 \cdot 7^4 \cdot 11^2 \cdot 13^3} \approx 0.069\,698\,255\,940 \tag{48}$$

is lower than all previously reported NSMs in 13 dimensions (most recently 0.071 035 [15], 0.070 974 [14], and 0.069 901 [16]).

As in 14 dimensions, we calculated the second moment matrix (4) to verify the condition $\boldsymbol{U} \propto \boldsymbol{I}_{13}$, which must be satisfied if the lattice is locally optimal. Surprisingly, it turned out that the second moment matrix is *not* proportional to the identity. Instead,

$$\boldsymbol{U} = \begin{bmatrix} \boldsymbol{W}_8 & \boldsymbol{0} \\ \boldsymbol{0} & \alpha \boldsymbol{I}_5 \end{bmatrix}, \tag{49}$$

where $\boldsymbol{W}_8$ is an 8×8 matrix with β on the diagonal and γ in all other components. The values of α, β, and γ are

$$\begin{aligned} \alpha &= \frac{3045475021549265414172665824642603505 11}{2^{81} \cdot 3^{10} \cdot 5^4 \cdot 7^4 \cdot 11^2 \cdot 13^2} &&\approx 0.069\,513, \\ \beta &= \frac{9787631469390979346380560690239381767}{2^{83} \cdot 3^{10} \cdot 5 \cdot 7^4 \cdot 11^2 \cdot 13^2} &&\approx 0.069\,814, \\ \gamma &= -\frac{9725744147275568174489190984115985 77}{2^{83} \cdot 3^{10} \cdot 5^4 \cdot 7^4 \cdot 11^2 \cdot 13^2} &&\approx -0.000\,055. \end{aligned} \tag{50}$$

This proves that L'_{13} generated by (47) is *not* the optimal 13-dimensional lattice quantizer and the identification method in [21] had failed for the first time. However, the fact that $\alpha - \beta$ and γ are near zero suggests that a local optimum might be nearby.

B. Optimization of the NSM

To find the local optimum near L'_{13}, we apply the algorithm of Sec. IV. The linearized perturbation matrix as a function of the step size ϵ is $\boldsymbol{A}_\epsilon = \boldsymbol{I}_n - \epsilon \bar{\boldsymbol{U}}$, with $\bar{\boldsymbol{U}}$ given by (21) and $\boldsymbol{U}$ by (49). The perturbed generator matrix is

$$\begin{aligned} \boldsymbol{B}'_{13} \boldsymbol{A}_\epsilon &= \boldsymbol{B}'_{13} \left(\boldsymbol{I}_n - \epsilon \left(\boldsymbol{U} - \frac{\operatorname{tr} \boldsymbol{U}}{n} \boldsymbol{I}_n \right) \right) && (51) \\ &= \left(1 + \frac{\epsilon \operatorname{tr} \boldsymbol{U}}{n} \right) \boldsymbol{B}'_{13} - \epsilon \boldsymbol{B}'_{13} \boldsymbol{U} && (52) \\ &= \left(1 + \frac{\epsilon}{13} (5\alpha + 8\beta) \right) \boldsymbol{B}'_{13} - \epsilon \boldsymbol{B}'_{13} \boldsymbol{U} && (53) \end{aligned}$$

and the perturbed second moment matrix is

$$\begin{aligned} \boldsymbol{A}_\epsilon^T \boldsymbol{U} \boldsymbol{A}_\epsilon &= \boldsymbol{U} - \epsilon(\bar{\boldsymbol{U}} \boldsymbol{U} + \boldsymbol{U} \bar{\boldsymbol{U}}) + \epsilon^2 \bar{\boldsymbol{U}} \boldsymbol{U} \bar{\boldsymbol{U}} && (54) \\ &= \begin{bmatrix} \boldsymbol{W}'_8 & \boldsymbol{0} \\ \boldsymbol{0} & \alpha' \boldsymbol{I}_5 \end{bmatrix} + O(\epsilon^2), && (55) \end{aligned}$$

where $\boldsymbol{W}'_8$ has β' in the diagonal and γ' in all other components. The values of these components as functions of ϵ are

$$\begin{aligned} \alpha' &= \alpha + \frac{16\alpha(\beta - \alpha)}{13} \epsilon, && (56) \\ \beta' &= \beta - \frac{2(5\beta^2 + 91\gamma^2 - 5\alpha\beta)}{13} \epsilon, && (57) \\ \gamma' &= \gamma + \frac{2\gamma(5\alpha - 18\beta - 78\gamma)}{13} \epsilon, && (58) \end{aligned}$$

which can be verified by inserting (49) (with $\boldsymbol{W}_8$ written in terms of β and γ) and (21) into (54) and keeping the terms up to linear order in ϵ.

We choose ϵ so that $\boldsymbol{A}_\epsilon^T \boldsymbol{U} \boldsymbol{A}_\epsilon \propto \boldsymbol{I}_{13}$ is approximately satisfied. Imposing $\gamma' = 0$ in (58) yields

$$\epsilon = \epsilon_1 \triangleq \frac{13}{2(-5\alpha + 18\beta + 78\gamma)} \approx 7.1843, \tag{59}$$

whereas imposing $\alpha' = \beta'$ using (56)–(57) yields

$$\epsilon = \epsilon_2 \triangleq \frac{13(\beta - \alpha)}{2(-8\alpha^2 + 3\alpha\beta + 5\beta^2 + 91\gamma^2)} \approx 7.1735. \tag{60}$$

Because $\boldsymbol{U}$ (49) is very close to a scaled identity, $\bar{\boldsymbol{U}}$ is very close to zero. Therefore, even with $\epsilon \approx 7$, all entries in $\epsilon \bar{\boldsymbol{U}}$ are less than 0.0014. That $\epsilon_1 \neq \epsilon_2$ means that the second moment matrix $\boldsymbol{A}_\epsilon^T \boldsymbol{U} \boldsymbol{A}_\epsilon$ of the deformed Voronoi region $\Omega \boldsymbol{A}_\epsilon$ will not be proportional to $\boldsymbol{I}_{13}$ for any ϵ. Hence, the multiplication with $\boldsymbol{A}_\epsilon$ likely cannot bring the lattice directly into a local minimum for any ϵ. Nevertheless, it is remarkable that both ϵ_1 and ϵ_2 satisfy $\gamma' \approx 0$ and $\alpha' \approx \beta'$. This confirms that $\boldsymbol{A}_\epsilon$ deforms the Voronoi region to a good approximation in the direction of a second moment matrix proportional to $\boldsymbol{I}_{13}$, which is hopefully sufficient to identify the optimal phase.

We will now show that the perturbation using $\boldsymbol{A}_\epsilon$ generates a *generalized glued lattice,* as defined in Sec. II-E. To this end, we generalize $\boldsymbol{B}'_{13}$ by gluing $\bar{L}^\times = a_1 A_7 \times a_2 D_5 \times a_3 \sqrt{2}\mathbb{Z}$ for arbitrary positive scale factors $\boldsymbol{a} = [a_1, a_2, a_3]$, instead of

gluing $A_7 \times D_5 \times \sqrt{2}\mathbb{Z}$ as in (47). This yields

$$\boldsymbol{B}_{13}(\boldsymbol{a}) = \left[\begin{array}{cccccccc:cccccc} -a_1 & a_1 & 0 & 0 & 0 & 0 & 0 & 0 & 0 & 0 & 0 & 0 & 0 \\ -a_1 & 0 & a_1 & 0 & 0 & 0 & 0 & 0 & 0 & 0 & 0 & 0 & 0 \\ -a_1 & 0 & 0 & a_1 & 0 & 0 & 0 & 0 & 0 & 0 & 0 & 0 & 0 \\ -a_1 & 0 & 0 & 0 & a_1 & 0 & 0 & 0 & 0 & 0 & 0 & 0 & 0 \\ -a_1 & 0 & 0 & 0 & 0 & a_1 & 0 & 0 & 0 & 0 & 0 & 0 & 0 \\ -a_1 & 0 & 0 & 0 & 0 & 0 & a_1 & 0 & 0 & 0 & 0 & 0 & 0 \\ -a_1 & 0 & 0 & 0 & 0 & 0 & 0 & a_1 & 0 & 0 & 0 & 0 & 0 \\ \hdashline 0 & 0 & 0 & 0 & 0 & 0 & 0 & 0 & 2a_2 & 0 & 0 & 0 & 0 \\ 0 & 0 & 0 & 0 & 0 & 0 & 0 & 0 & a_2 & a_2 & 0 & 0 & 0 \\ 0 & 0 & 0 & 0 & 0 & 0 & 0 & 0 & a_2 & 0 & a_2 & 0 & 0 \\ 0 & 0 & 0 & 0 & 0 & 0 & 0 & 0 & a_2 & 0 & 0 & a_2 & 0 \\ 0 & 0 & 0 & 0 & 0 & 0 & 0 & 0 & a_2 & 0 & 0 & 0 & a_2 \\ \hdashline b & b & b & b' & b' & b' & b' & b' & \frac{a_2}{2} & \frac{a_2}{2} & \frac{a_2}{2} & \frac{a_2}{2} & \frac{a_2}{2} \end{array}\right], \tag{61}$$

where $b \triangleq (10a_1 + a_3)/16$ and $b' \triangleq b - a_1$.

The first seven rows of $\boldsymbol{B}_{13}(\boldsymbol{a})$ generate $a_1 A_7$ (embedded in $\mathbb{R}^8$) and the next five rows generate $a_2 D_5$. The third component lattice $a_3\sqrt{2}\mathbb{Z}$ consists of all multiples of $a_3[1\ 1\ 1\ 1\ 1\ 1\ 1\ 1\ 0\ 0\ 0\ 0\ 0]/2$ and is orthogonal to the first twelve rows. That this vector belongs to the lattice can be seen by taking 8 times the last row of (61) and adding or subtracting suitable multiples of the other rows. Indeed, if the last row of (61) would be replaced by $a_3[1\ 1\ 1\ 1\ 1\ 1\ 1\ 1\ 0\ 0\ 0\ 0\ 0]/2$, then the resulting matrix would generate the (unglued) product lattice $\bar{L}^\times$.

Constructed from the product lattice, the glued lattice is L_{13} of the form L_{gl}^{g} given by (17) with $L = \bar{L}^\times$ and glue group $\Gamma^{\text{g}} = \{i\boldsymbol{g}_1 \colon i = 0, \dots, 7\}$, where $\boldsymbol{g}_1$ is the last row of (61). Interestingly, Γ^{g} is not a subgroup of $(\bar{L}^\times)^*/\bar{L}^\times$, not even for $a_1 = a_2 = a_3 = 1$.

The glued lattice L_{13}, like its constituent product lattice $\bar{L}^\times$, has 56 vectors of length $a_1\sqrt{2}$, belonging to $a_1 A_7$, 40 vectors of length $a_2\sqrt{2}$, belonging to $a_2 D_5$, and 2 vectors of length $a_3\sqrt{2}$, belonging to $a_3\sqrt{2}\mathbb{Z}$. The shortest nonzero vectors have length $\min(a_1, a_2, a_3)\sqrt{2}$, and so the number of those vectors depends on the parameter values. The kissing number can thus be 98 (for $a_1 = a_2 = a_3$), 96, 58, 56, 42, 40, or 2 (for $a_3 < \min(a_1, a_2)$).

As a special case, $\boldsymbol{B}'_{13}$ in (47) is obtained by setting $\boldsymbol{a} = [1, 1, 1]$ in (61). Another special case of (61) is $\boldsymbol{B}'_{13}\boldsymbol{A}_\epsilon$ in (53) for any ϵ, which can be verified by setting

$$a_1 = 1 - \frac{5\beta - 5\alpha - 13\gamma}{13}\epsilon, \tag{62}$$

$$a_2 = 1 + \frac{8\beta - 8\alpha}{13}\epsilon, \tag{63}$$

$$a_3 = 1 - \frac{5\beta - 5\alpha + 91\gamma}{13}\epsilon \tag{64}$$

in (61) and comparing the result component-wise with (53). We therefore conjecture that the optimal 13-dimensional lattice has the form (61) for some $\boldsymbol{a}$. We do not constrain $\boldsymbol{a}$ to the single degree of freedom given by (62)–(64), because of the approximations involved in deriving those relations. On the other hand, it is unnecessary to consider the whole three-dimensional parameter space $\boldsymbol{a} = [a_1, a_2, a_3]$, because rescaling the lattice by a nonzero constant c does not affect the NSM (2) and $c\boldsymbol{B}_{13}(\boldsymbol{a}) = \boldsymbol{B}_{13}(c\boldsymbol{a})$. We therefore fix $a_1 = 1$ without loss of generality.

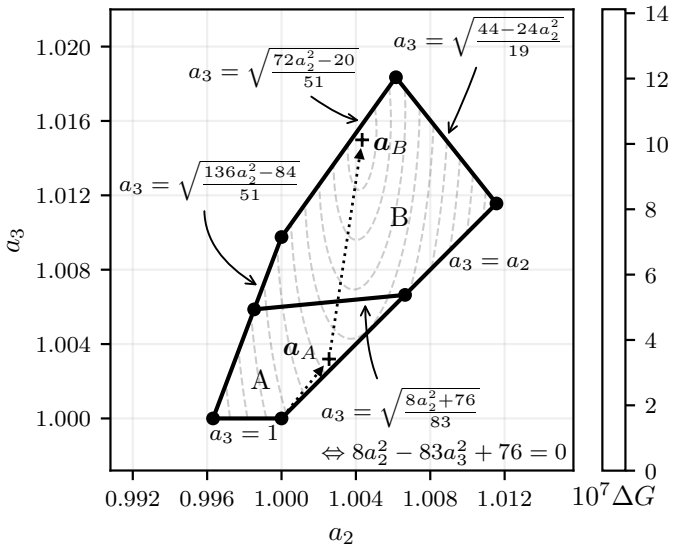

Fig. 5. Phases A and B of the lattice (61). Solid lines show phase boundaries where 1-face lengths vanish and the dots mark the points where lines of vanishing 1-face lengths intersect. The color gradient indicates the value of $\Delta G(\boldsymbol{a}) \triangleq G(\boldsymbol{a}) - G(\boldsymbol{a}_{\text{opt}})$, where $G = G_A$ in phase A, $G = G_B$ in phase B, and $G(\boldsymbol{a}_{\text{opt}})$ is given in (69). Dashed lines show contours of equal G. The contours connect between phases A and B (since $G_A = G_B$ there) and have derivatives that match across the phase boundary, up to the 13th order, but they are *not* infinitely differentiable. See also [21, Sec. III-B]. The apparent smoothness is due to the functions G_B and G_A being extremely similar throughout the colored region (see (66) and (71)). The dotted arrows indicate the search path described in Sec. VI-B. The minimum of G lies very close to $\boldsymbol{a}_B$ (see (72)).

We analyze the parametric lattice first at the point $\boldsymbol{a}_A = [1, a_2^A, a_3^A]$, where

$$\begin{aligned} a_2^A &= 392/391 \approx 1.002\,558, \\ a_3^A &= 314/313 \approx 1.003\,195. \end{aligned} \tag{65}$$

These values were obtained by setting $\epsilon = \epsilon_1$ in (62)–(64), normalizing $\boldsymbol{a}$ by a_1, and using rational approximations to facilitate symbolic calculations. We call the phase that $\boldsymbol{a}_A$ lies in *phase A*. Fig. 5 shows $\boldsymbol{a}_A$ and the phase boundaries identified by vanishing lengths of 1-faces. The additional conditions (i)–(iv) of Sec. III are verified as well. Note that not all phase boundaries are straight lines, as can be seen from the expressions defining the boundaries in Fig. 5.

The NSM G_A of phase A as a function of $\boldsymbol{a}$ is given in Appendix A. To locate a minimum of G_A, we use $G_2^A \triangleq \partial G_A/\partial a_2$ and $G_3^A \triangleq \partial G_A/\partial a_3$. A local minimum of G_A in $\boldsymbol{a}$ must have $G_2^A = G_3^A = 0$. However, no such point exists within phase A. We therefore need to repeat the analysis for another phase.

According to the iterative strategy outlined in Sec. IV, the next point to analyze is the local minimum of $G_A(\boldsymbol{a})$ closest to (with respect to the Euclidean distance in parameter space) phase A. It is located at $\boldsymbol{a}_B \approx [1, 1.004\,336, 1.014\,983]$.[5] Note that $G_A(\boldsymbol{a}_B)$ is not the NSM of $\boldsymbol{B}_{13}(\boldsymbol{a}_B)$, but it is the best approximation available at this point of the analysis. The phase determined from constructing the Voronoi region at $\boldsymbol{a}_B$ is also shown in Fig. 5, with exact expressions for the boundaries given in the figure. We call this *phase B*. The criteria (i)–(iv) of Sec. III are satisfied within both phases.

The NSM in phase B is, still assuming $a_1 = 1$,

$$G_B(\boldsymbol{a}) = G_A(\boldsymbol{a}) + \frac{\left(8a_2^2 - 83a_3^2 + 76\right)^{14}}{2^{78}\cdot 3^5\cdot 5^3\cdot 7^2\cdot 11\cdot 13^2\ V(\boldsymbol{a})^{2+2/13}}, \tag{66}$$

where $V(\boldsymbol{a}) = |\det \boldsymbol{B}_{13}(\boldsymbol{a})| = a_2^5 a_3$. Therefore, the NSM $G(\boldsymbol{a})$ of (61), which equals $G_A(\boldsymbol{a})$ in phase A and $G_B(\boldsymbol{a})$ in phase B, is 13 (but not 14) times differentiable on the boundary between the two phases, which is given by $8a_2^2 - 83a_3^2 + 76 = 0$. This observation demonstrates that G_A is a good approximation of G also outside phase A, which in turn justifies the strategy of taking the minimum of G_A as the next point to analyze also when it lies outside phase A.

The minimum of $G_B(\boldsymbol{a})$ is located at the only common root of

$$G_2^B \triangleq \frac{\partial G_B}{\partial a_2} \quad \text{and} \quad G_3^B \triangleq \frac{\partial G_B}{\partial a_3} \tag{67}$$

in the interior of phase B. The two equations $G_2^B = 0$ and $G_3^B = 0$ are equivalent to $f_2^B = 0$ and $f_3^B = 0$, where f_i^B are rational polynomials of degree 14 in $v_2 \triangleq a_2^2$ and $v_3 \triangleq a_3^2$. They are obtained via

$$\begin{aligned} f_2^B(a_2^2, a_3^2) &\triangleq a_2^{\frac{153}{13}} a_3^{\frac{28}{13}} G_2^B(\boldsymbol{a}), \\ f_3^B(a_2^2, a_3^2) &\triangleq a_2^{\frac{140}{13}} a_3^{\frac{41}{13}} G_3^B(\boldsymbol{a}). \end{aligned} \tag{68}$$

Explicit expressions for f_2^B and f_3^B are given in the online supplementary material.

The minimum of G_B in phase B is shown in Fig. 5. Its value is

$$G(\boldsymbol{a}_{\text{opt}}) = G_B(\boldsymbol{a}_{\text{opt}}) \approx 0.069\,697\,638\,992, \tag{69}$$

where

$$\boldsymbol{a}_{\text{opt}} \approx [1,\ 1.004\,336\,185\,575,\ 1.014\,983\,466\,336]. \tag{70}$$

The minimum (69) is not far from the numerically estimated NSM $0.069\,696 \pm 0.000\,002$ [21, Tab. II]. This is slightly lower than the NSM (48) of the parametric lattice $\boldsymbol{B}'_{13} = \boldsymbol{B}_{13}(1,1,1)$. The lattice generated by $\boldsymbol{B}_{13}(\boldsymbol{a}_{\text{opt}})$ will be referred to as $\text{ADZ}_{13}^{\text{gl}}$.

[5] During this work, we analyzed the lattice at $[1, 1.004, 1.008]$ instead of $\boldsymbol{a}_B$ and only later realized that $\boldsymbol{a}_B$ would have been a better choice. Happily, both points are in the same phase and thus yield the same expression for G_B.

Interestingly, the difference between G_A and G_B at $\boldsymbol{a}_{\text{opt}}$ is much smaller than the range of variation of the NSM across phases A and B,

$$G_B(\boldsymbol{a}_{\text{opt}}) - G_A(\boldsymbol{a}_{\text{opt}}) \approx 1.8\cdot 10^{-31}. \tag{71}$$

Furthermore, the minima of G_A and G_B lie very close to each other, with a difference in parameters of only

$$\boldsymbol{a}_B - \boldsymbol{a}_{\text{opt}} \approx [0,\ 4\cdot 10^{-27},\ 9\cdot 10^{-26}]. \tag{72}$$

This further supports the assumption that the NSM behaves very similarly in neighboring phases. Based on this and the fact that the initial numerical search converged near $\boldsymbol{a}_{\text{opt}}$, we conjecture that (69) is the minimum NSM across all phases and hence that $\text{ADZ}_{13}^{\text{gl}}$, which is generated by $\boldsymbol{B}_{13}(\boldsymbol{a}_{\text{opt}})$, is the globally optimal lattice quantizer in 13 dimensions.

As in the 14-dimensional case, we also calculated the second moment matrix (4) of (61) in phase B as a function of $\boldsymbol{a}$. As expected from the result (49) for the nonparametric lattice (47), the second moment matrix is again of the form

$$\boldsymbol{U} = \begin{bmatrix} \boldsymbol{W}_8 & \boldsymbol{0} \\ \boldsymbol{0} & \alpha(\boldsymbol{a})\boldsymbol{I}_5 \end{bmatrix}, \tag{73}$$

where $\boldsymbol{W}_8$ is an 8×8 matrix with $\beta(\boldsymbol{a})$ on the diagonal and $\gamma(\boldsymbol{a})$ in all other components. The functions $\alpha(\boldsymbol{a})$, $\beta(\boldsymbol{a})$, and $\gamma(\boldsymbol{a})$ can be expressed as

$$\begin{aligned} \alpha(\boldsymbol{a}) &= V(\boldsymbol{a})^{\frac{2}{13}} G_B(\boldsymbol{a}) + \frac{13}{10V(\boldsymbol{a})^2} f_2^B(a_2^2, a_3^2), \\ \beta(\boldsymbol{a}) &= V(\boldsymbol{a})^{\frac{2}{13}} G_B(\boldsymbol{a}) - \frac{13}{16V(\boldsymbol{a})^2} f_2^B(a_2^2, a_3^2), \\ \gamma(\boldsymbol{a}) &= \frac{13}{112V(\boldsymbol{a})^2}\left[f_2^B(a_2^2, a_3^2) + 8 f_3^B(a_2^2, a_3^2)\right]. \end{aligned} \tag{74}$$

The condition $\boldsymbol{U} \propto \boldsymbol{I}_{13}$ is equivalent to $\alpha(\boldsymbol{a}) = \beta(\boldsymbol{a})$ and $\gamma(\boldsymbol{a}) = 0$, which in turn is equivalent to $f_2^B(a_2^2, a_3^2) = f_3^B(a_2^2, a_3^2) = 0$. Since f_2^B and f_3^B both vanish at $\boldsymbol{a}_{\text{opt}}$, the necessary condition $\boldsymbol{U} \propto \boldsymbol{I}_{13}$ for the lattice to be a locally optimal lattice quantizer is satisfied.

C. Further properties of the Voronoi region

The automorphism group $\text{Aut}(L_{13})$ of this lattice is much simpler to describe than $\text{Aut}(L_{14})$ in Sec. V-B. In terms of the lattice vectors $\boldsymbol{u}\boldsymbol{B}_{13}(\boldsymbol{a})$, where $\boldsymbol{B}_{13}(\boldsymbol{a})$ is given in (61) and $\boldsymbol{u} \in \mathbb{Z}^{13}$, the group consists of all permutations of the first eight components (8! symmetries), all permutations of the last five components (5! symmetries), an even number of sign changes among the last five components ($\binom{5}{0} + \binom{5}{2} + \binom{5}{4} = 16$ symmetries), and an overall sign change (2 symmetries). Together, these form the group $\text{Aut}(L_{13})$ of order $2\cdot 8!\cdot 5!\cdot 16 = 154\,828\,800$.

The Voronoi region of this lattice in phase B has 960 828 340 vertices, 5 454 facets, and in total 303 633 215 079 faces across all dimensions from 0 to 13. Tab. I lists these values as well as the number of faces and face classes in dimensions 0 through 13 for $\boldsymbol{B}'_{13}$ and $\boldsymbol{B}_{13}(\boldsymbol{a})$ in phases A and B.

The theta images of $\boldsymbol{B}'_{13}$ and $\boldsymbol{B}_{13}(\boldsymbol{a}_{\text{opt}})$ are shown in Fig. 6. The 98 shortest nonzero vectors of $\boldsymbol{B}'_{13}$, which were

TABLE I
NUMBER OF FACES AND FACE CLASSES OF THE LATTICE (61) AT $a_2 = a_3 = 1$ COMPARED WITH PHASES A AND B.

	$a_2 = a_3 = 1$		phase A		phase B	
dim.	faces	classes	faces	classes	faces	classes
0	913 062 580	2 380	961 419 700	2 429	960 828 340	2 444
1	8 323 478 208	10 402	8 510 132 928	10 561	8 504 452 288	10 606
2	31 111 318 496	21 388	31 451 395 296	21 636	31 432 418 016	21 693
3	64 038 899 360	29 081	64 426 365 600	29 334	64 395 704 480	29 373
4	81 053 843 332	29 948	81 353 017 732	30 139	81 326 693 252	30 148
5	66 158 634 484	24 433	66 317 190 644	24 550	66 305 273 844	24 546
6	35 348 681 664	16 073	35 404 233 664	16 130	35 401 671 104	16 122
7	12 255 202 196	8 571	12 266 760 596	8 590	12 266 563 476	8 586
8	2 670 432 810	3 691	2 671 508 010	3 694	2 671 508 010	3 694
9	343 917 632	1 266	343 917 632	1 266	343 917 632	1 266
10	23 483 364	343	23 483 364	343	23 483 364	343
11	695 818	71	695 818	71	695 818	71
12	5 454	10	5 454	10	5 454	10
13	1	1	1	1	1	1
total	302 241 655 399	147 658	303 730 126 439	148 754	303 633 215 079	148 903

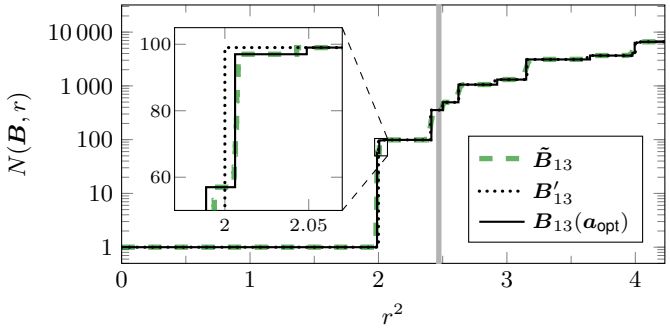

Fig. 6. Theta image of the suboptimal $\boldsymbol{B}'_{13}$ and the conjectured optimal $\boldsymbol{B}_{13}(\boldsymbol{a}_{\text{opt}})$, both rescaled to determinant 1 and superimposed on the theta image of the numerically optimized lattice in Fig. 4. The inset is in linear scale to better visualize the three steps at $r^2 = 1.99$, 2.01, and 2.05. The two shells to the left of the gray bar were used to determine $\boldsymbol{B}'_{13}$.

mentioned after (61), split into three classes of vectors in $\boldsymbol{B}_{13}(\boldsymbol{a})$, with squared norms $2a_1^2$, $2a_2^2$, and $2a_3^2$, and orbit lengths 56, 40, and 2, respectively. The step from 1 to 99 at $r^2 = 2$ in the theta image of $\boldsymbol{B}'_{13}$ corresponds to three stacked steps for $\boldsymbol{B}_{13}(\boldsymbol{a}_{\text{opt}})$, at $r^2 = 1.99$, 2.01, and 2.05, respectively. This explains why the lattice identification method in [21] failed for $\tilde{\boldsymbol{B}}_{13}$. The method cannot distinguish between a single lattice shell with numerical fluctuations and several closely-spaced shells.

Some properties of this parametric lattice change nontrivially even within a phase, i.e., without occurring together with a change of the topology of Ω. For example, the kissing number in both phases A and B is

$$\tau = \begin{cases} 56 & a_2 > 1, \\ 96 & a_2 = 1, \\ 40 & a_2 < 1, \end{cases} \tag{75}$$

still assuming $a_1 = 1$. (It is 2, 40, 42, 56, 58, and 98 in different phases just south of phase A, i.e., for $a_3 \le \max(1, a_2)$.)

Accordingly, the packing radius and packing density in phases A and B are, respectively,

$$\rho = \frac{\min(1, a_2)}{\sqrt{2}}, \qquad \Delta = \frac{128\pi^6\rho^{13}}{135135 a_2^5 a_3}. \tag{76}$$

At $\boldsymbol{a}_{\text{opt}}$ in phase B, we get $\rho \approx 0.707\,107$ and $\Delta \approx 0.009\,700$.

The covering radius R and covering thickness Θ in both phases are

$$R = \frac{\sqrt{2}\sqrt{64a_2^4 + 48a_2^2a_3^2 - 64a_2^2 + 9a_3^4 - 8a_3^2 + 144}}{16}, \qquad \Theta = \frac{128\pi^6 R^{13}}{135135 a_2^5 a_3} \tag{77}$$

Their respective numerical values at $\boldsymbol{a}_{\text{opt}}$ in phase B are $R \approx 1.236\,648$ and $\Theta \approx 13.889\,470$.

The highest known lattice packing density and lowest known lattice covering thickness in dimension 13 are, respectively, $\Delta(K_{13}) \approx 0.029\,208$ [1, Tab. 1.2] and $\Theta(\mathsf{L}^{\text{c}}_{13}) \approx 7.762\,108$ [30, Tab. 2].

D. Exploring the phase structure

Phases A and B of the lattice, shown in Fig. 5, already show an intricate geometry, with some boundaries consisting of curved lines. One can gain an insight into the neighboring phases by looking for lines of vanishing 1-face lengths in the face hierarchy of a certain phase evaluated at parameters *outside* its phase. If those 1-faces are still part of the Voronoi region, then their vanishing does indeed indicate a phase boundary. In fact, phase B can be completely characterized by vanishing lengths of 1-faces in phase A and vice versa. Fig. 7 shows the curves along which lengths of 1-faces of the Voronoi region in phase B become zero. Semitransparent curves are drawn for each class of 1-faces, so that darker curves indicate a larger number of 1-face classes with vanishing lengths. These

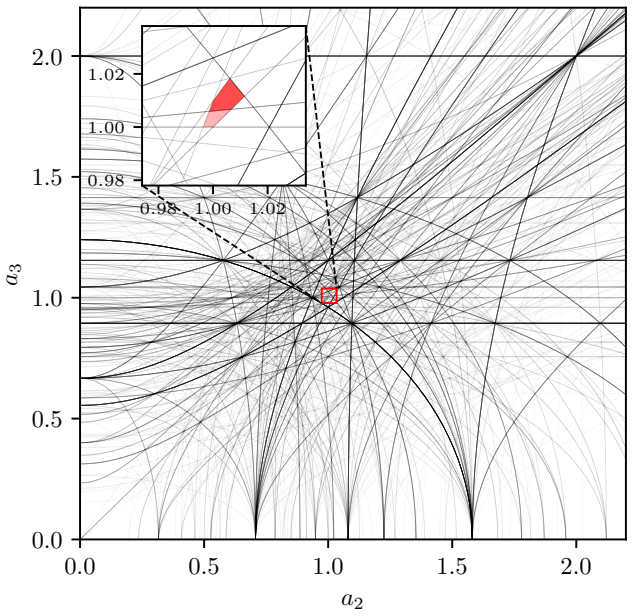

Fig. 7. Lines where lengths of 1-faces in phase B become zero. The lighter and darker shaded regions in the inset show phases A and B from Fig. 5, respectively. Note that these lines may not accurately capture the phase transitions of $\boldsymbol{B}_{13}(\boldsymbol{a})$ outside phases A and B.

results should be interpreted as suggestive of the complexity of the *phase landscape*. More robust pictures can be made by constructing the Voronoi region for multiple points in the (a_2, a_3)-plane and comparing the resulting phase landscapes.

VII. Discussion and Conclusions

By combining several analysis methods, we obtain new lattice quantizers in dimensions 13 and 14, which have the lowest NSMs reported in those dimensions. The key steps are to first find an approximate lattice using stochastic gradient descent. This is followed by the exact identification as a generalized glued product lattice. The second moment matrix then provides a clue whether further refinement is necessary, which was an important step in the analysis of the 13-dimensional lattice. Parameterizing the product lattice by scaling the components has proved to be a successful route. The optimal parameters are determined via the common root of two polynomials of degree 14 (in dimension 13) and a root of a single polynomial of degree 15 (in dimension 14).

We conjecture these two lattices to be optimal based on the following rationale. Finding the globally optimal lattice quantizer can be broken up into three separate problems: (i) identifying a lattice close to[6] and with the same symmetry group as the global optimum (which we assume to be a highly symmetric lattice), (ii) finding a parametrization of this lattice such that the optimum is one of the lattices in this family, and (iii) finding the exact parameters of the optimum. If these problems are solved, then the globally optimal lattice quantizer has been found.

[6]With *close* we mean that there exist equivalent lattices whose generator matrices differ only within the accuracy of the SGD searches.

TABLE II
Conjectured optimal lattices

dim.	lattice	generator matrix	exact parameters	numerical parameters
13	$\mathrm{ADZ}_{13}^{\mathrm{gl}}$	(61)	$a_1 = 1$, $a_2 = \sqrt{v_{2,0}}$, $a_3 = \sqrt{v_{3,0}}$, where $[v_{2,0}, v_{3,0}]$ is the common root of f_2^B, f_3^B closest to $[1, 1]$ (see (78), (66)–(68))	$a_1 = 1$ $a_2 = 1.004\,336\ldots$ $a_3 = 1.014\,983\ldots$
14	$\mathrm{K'D}_{14}^{\mathrm{gl}}$	(22)	$a = \sqrt{v_0}$, where v_0 is the second positive root of (40)	$a = 1.314\,224\ldots$

An argument that problem (i) is solved is the following. We performed 100 SGD searches in [21], many of which converged close to the smallest NSM obtained. Since the corresponding lattices are close to each other, it is plausible that the global optimum also lies close to them. If true, the global optimum is attained for a small deformation of one of the numerical generator matrices (or one equivalent to it). We believe that the glued product structures we found are the only highly symmetric ones attainable from the numerical lattices by small deformations, in which case problem (i) is solved.[7]

We argue that problem (ii) is solved by the parametrizations we present in the 13- and 14-dimensional cases. They contain lattices that are very close to the numerical ones and additional parameters would either lead to equivalent lattices (e.g., rotation and scaling of the whole lattices), or to less symmetric lattices.

Problem (iii) is then solved by the algorithm in Sec. IV, which identifies the phase containing the optimum and locates it exactly. We are confident that this algorithm finds the *only* minimum in the vicinity of the numerical lattice as the NSM is very smooth across phase boundaries (derivatives of up to order 13 are continuous in the 13-dimensional case).

If the above conjecture is true, then the optimal lattice quantizers in dimensions 13 and 14 are those given in Tab. II.

A somewhat surprising result is that the optimal parameters in 13 dimensions are close but not equal to unity. At exactly 1, the lattice is not even locally optimal, since its second moment matrix is not proportional to the identity. The difference is insignificant in practice but demonstrates the elusive nature of optimal lattice quantizers. Furthermore, by visualizing the points in parameter space where lengths of 1-faces become zero (Fig. 7), we found that Voronoi regions can undergo a much higher number of topological changes than we initially expected.

Together with the conjectured optimal lattices in dimensions below 13 and in dimension 16 [1, Chap. 1], [20], [21], we believe that the list of optimal lattice quantizers is now complete up to dimension 16.

[7]Problems (ii) and (iii) may be skipped if a highly symmetric lattice with no undetermined parameters is obtained by small deformations of a numerical generator and this lattice has white quantization noise. However, the argument becomes stronger if (ii) and (iii) are also solved.

APPENDIX A
EXACT NSM IN DIMENSION 13

The NSM of the two-parameter lattice (61) with $a_1 = 1$ in phase A (see Fig. 5) is

$$G_A(\boldsymbol{a}) = \frac{\sum_{i=0}^{14}\sum_{j=0}^{14-i} c_{i,j} a_2^{2i} a_3^{2j}}{2^{81}\cdot 3^{10}\cdot 5^4\cdot 7^4\cdot 11^2\cdot 13^3\ V(\boldsymbol{a})^{2+2/n}}, \tag{78}$$

where $V(\boldsymbol{a}) = a_2^5 a_3$ and $n = 13$. The coefficients $c_{i,j}$ are integers given in Tab. III.

APPENDIX B
PROOFS OF EQUIVALENCES

Two lattices with Gram matrices $\boldsymbol{A}$ and $\boldsymbol{A}'$ are equivalent if and only if there exists a real positive scalar c and an integer matrix $\boldsymbol{U}$ with determinant ± 1 such that

$$\boldsymbol{A}' = c\boldsymbol{U}\boldsymbol{A}\boldsymbol{U}^{\mathrm{T}}. \tag{79}$$

To determine if two given lattices are equivalent is a non-trivial task. In this appendix, we prove hitherto unknown equivalences between known lattices, which were discovered during this work and are mentioned in the text. The search for constructive mapping rules between different lattice representations was facilitated by a heuristic algorithm that selects a set of short vectors in each lattice and attempts to map the sets onto each other.

A. Equivalence between three 10-dimensional lattices

It was claimed in Sec. V-A that the top-left 10×10 submatrix of $\boldsymbol{B}_{14}(\boldsymbol{a})$ generates a lattice that is equivalent to both K_{10}' in [26, Sec. 8.5] and the lattice with automorphism group $(C_6 \times \mathrm{SU}_4(2)) : C_2$ in [27]. Gram matrices of the two latter are available in the online Catalogue of Lattices [28] under the labels *KAPPA10′* and *(C6 x SU(4,2)):C2*, respectively, as

$$\boldsymbol{A}_1 = \begin{bmatrix}
4 & -2 & -2 & 1 & 1 & 1 & -1 & -1 & -2 & -2\\
-2 & 4 & 1 & -2 & -2 & -2 & -1 & -1 & 1 & 1\\
-2 & 1 & 4 & -2 & -2 & -2 & 0 & 0 & 2 & 0\\
1 & -2 & -2 & 4 & 1 & 1 & 0 & 0 & -1 & 0\\
1 & -2 & -2 & 1 & 4 & 1 & 0 & 0 & -2 & -1\\
1 & -2 & -2 & 1 & 1 & 4 & 2 & 2 & 0 & 0\\
-1 & -1 & 0 & 0 & 0 & 2 & 4 & 1 & 0 & 0\\
-1 & -1 & 0 & 0 & 0 & 2 & 1 & 4 & 2 & 2\\
-2 & 1 & 2 & -1 & -2 & 0 & 0 & 2 & 4 & 1\\
-2 & 1 & 0 & 0 & -1 & 0 & 0 & 2 & 1 & 4
\end{bmatrix}, \tag{80}$$

$$\boldsymbol{A}_2 = \begin{bmatrix}
4 & 1 & 1 & -2 & 1 & -2 & -2 & -2 & 2 & -2\\
1 & 4 & 0 & -1 & 2 & 1 & 0 & 0 & 2 & -2\\
1 & 0 & 4 & 1 & 2 & -2 & 1 & 1 & 2 & 1\\
-2 & -1 & 1 & 4 & -1 & 1 & 2 & 1 & -1 & 2\\
1 & 2 & 2 & -1 & 4 & -1 & 1 & 1 & 2 & 0\\
-2 & 1 & -2 & 1 & -1 & 4 & 0 & 1 & -1 & 0\\
-2 & 0 & 1 & 2 & 1 & 0 & 4 & 2 & -1 & 1\\
-2 & 0 & 1 & 1 & 1 & 1 & 2 & 4 & -1 & 2\\
2 & 2 & 2 & -1 & 2 & -1 & -1 & -1 & 4 & -1\\
-2 & -2 & 1 & 2 & 0 & 0 & 1 & 2 & -1 & 4
\end{bmatrix}. \tag{81}$$

If $\boldsymbol{B}_3$ denotes the top-left 10×10 submatrix of $\boldsymbol{B}_{14}(\boldsymbol{a})$ in (22), then the equivalences can be explicitly shown as

$$\boldsymbol{B}_3\boldsymbol{B}_3^{\mathrm{T}} = \boldsymbol{U}_1\boldsymbol{A}_1\boldsymbol{U}_1^{\mathrm{T}} = \boldsymbol{U}_2\boldsymbol{A}_2\boldsymbol{U}_2^{\mathrm{T}} \tag{82}$$

with

$$\boldsymbol{U}_1 = \begin{bmatrix}
1 & 0 & 0 & 0 & 0 & 0 & 0 & 0 & 0 & 0\\
1 & 1 & 0 & 0 & 0 & 0 & 0 & 0 & 0 & 0\\
1 & 1 & 1 & 1 & 0 & 0 & 1 & 0 & 0 & 0\\
1 & 1 & 0 & 1 & 0 & -1 & 1 & 1 & 0 & 0\\
-1 & -1 & 0 & 0 & -1 & 0 & -1 & 0 & -1 & 0\\
-2 & -1 & -1 & 0 & -1 & 0 & -1 & 0 & -1 & -1\\
1 & 0 & 1 & 0 & 0 & 0 & 0 & 0 & 0 & 0\\
1 & 1 & 1 & 1 & 0 & 0 & 0 & 0 & 0 & 0\\
0 & -1 & 0 & 0 & -1 & 0 & 0 & 0 & 0 & 0\\
0 & -1 & -1 & 0 & -1 & -1 & 0 & 0 & 0 & 0
\end{bmatrix}, \tag{83}$$

$$\boldsymbol{U}_2 = \begin{bmatrix}
1 & 0 & 0 & 0 & 0 & 0 & 0 & 0 & 0 & 0\\
0 & 0 & 0 & 0 & 0 & 0 & 0 & 0 & 1 & 0\\
0 & -1 & 0 & 0 & 1 & 0 & 0 & 0 & 0 & 0\\
1 & -1 & -1 & 0 & 0 & 0 & 1 & 1 & 1 & 0\\
0 & -1 & -1 & 0 & 0 & 0 & 0 & 0 & 1 & 0\\
0 & 0 & 1 & -2 & -1 & 1 & 1 & -1 & 0 & 1\\
0 & 0 & -1 & 1 & 1 & -1 & -1 & 0 & 0 & 0\\
0 & -1 & -1 & 0 & 1 & 0 & 0 & 0 & 1 & 0\\
1 & -1 & -1 & 1 & 1 & 0 & 0 & 0 & 0 & 0\\
1 & -1 & -1 & 0 & 0 & 0 & 1 & 0 & 1 & 0
\end{bmatrix}. \tag{84}$$

B. Equivalence between three 12-dimensional lattices

It was claimed in Sec. I that the best 12-dimensional lattices in [13] and [14] are equivalent. Here we prove this equivalence, and also that the two best 12-dimensional lattices in [13, Tab. III] are equivalent to each other. Generator matrices for these two are

$$\boldsymbol{B}_4 = \begin{bmatrix}
2 & 0 & 0 & 0 & 0 & 0 & 0 & 0 & 0 & 0 & 0 & 0\\
0 & 2 & 0 & 0 & 0 & 0 & 0 & 0 & 0 & 0 & 0 & 0\\
0 & 0 & 2 & 0 & 0 & 0 & 0 & 0 & 0 & 0 & 0 & 0\\
0 & 0 & 0 & 2 & 0 & 0 & 0 & 0 & 0 & 0 & 0 & 0\\
0 & 0 & 0 & 0 & 2 & 0 & 0 & 0 & 0 & 0 & 0 & 0\\
0 & 0 & 0 & 0 & 0 & 2 & 0 & 0 & 0 & 0 & 0 & 0\\
1 & 1 & 1 & 0 & 0 & 1 & 0 & 1 & 0 & 0 & 0 & 0\\
0 & 0 & 1 & 1 & 1 & 0 & 0 & 1 & 0 & 1 & 0 & 0\\
0 & 0 & 0 & 0 & 1 & 1 & 1 & 0 & 0 & 1 & 0 & 1\\
0 & 1 & 0 & 0 & 0 & 0 & 1 & 1 & 1 & 0 & 0 & 1\\
0 & 1 & 0 & 1 & 0 & 0 & 0 & 0 & 1 & 1 & 1 & 0\\
1 & 0 & 0 & 1 & 0 & 1 & 0 & 0 & 0 & 0 & 1 & 1
\end{bmatrix}, \tag{85}$$

$$\boldsymbol{B}_5 = \begin{bmatrix}
2 & 0 & 0 & 0 & 0 & 0 & 0 & 0 & 0 & 0 & 0 & 0\\
0 & 2 & 0 & 0 & 0 & 0 & 0 & 0 & 0 & 0 & 0 & 0\\
0 & 0 & 2 & 0 & 0 & 0 & 0 & 0 & 0 & 0 & 0 & 0\\
0 & 0 & 0 & 2 & 0 & 0 & 0 & 0 & 0 & 0 & 0 & 0\\
0 & 0 & 0 & 0 & 2 & 0 & 0 & 0 & 0 & 0 & 0 & 0\\
0 & 0 & 0 & 0 & 0 & 2 & 0 & 0 & 0 & 0 & 0 & 0\\
1 & 1 & 1 & 1 & 1 & 1 & 1 & 0 & 1 & 1 & 0 & 0\\
0 & 0 & 1 & 1 & 1 & 1 & 1 & 1 & 1 & 0 & 1 & 1\\
1 & 1 & 0 & 0 & 1 & 1 & 1 & 1 & 1 & 1 & 1 & 0\\
1 & 0 & 1 & 1 & 0 & 0 & 1 & 1 & 1 & 1 & 1 & 1\\
1 & 1 & 1 & 0 & 1 & 1 & 0 & 0 & 1 & 1 & 1 & 1\\
1 & 1 & 1 & 1 & 1 & 0 & 1 & 1 & 0 & 0 & 1 & 1
\end{bmatrix}, \tag{86}$$

TABLE III
COEFFICIENTS OF (78).

i	j	$c_{i,j}$	i	j	$c_{i,j}$
0	0	23703209706893343661679973557600256 0	4	6	10746939583906574548738535482571882496 00
0	1	−14632076264609828558617705939667517 44	4	7	28583892500513897616297638686689853440 0
0	2	59348988572086834737795164709972869 12	4	8	10233818162758930242626624773049057280 0
0	3	−62067644162040813359452576549835898 88	4	9	34784275308690432469536266656562380800
0	4	32507564456634516864945128503037132 80	4	10	71765698838121370579573848424260608 00
0	5	27531155233952148807494665749780758528	5	0	−48938510276002640981506686191547711 4880
0	6	−52726816487909003990881825349185634304	5	1	−34985541070033854268879949743484043 2640
0	7	78104448955066346519712454831909502976	5	2	−45941842468973104635380247198181294 0800
0	8	−69925347164027747089931918702597099520	5	3	−71900510546295609832666679417658094387 20
0	9	48611866333961358524429289555671840768	5	4	−58303281953219042705140916892963805593 60
0	10	−23998790238070057635922084475102183168	5	5	−30690294082869477733302414921447348633 60
0	11	86727314173237146577535144144902545 92	5	6	−11907308170025435652273963632317956096 00
0	12	−20751590915797676126213327304091693 60	5	7	−32031663214821712820447618002046681088 0
0	13	32205223925144888219199601129647757 6	5	8	−10313590710707483469312944692773126144 0
0	14	−17556504634521010054008849438439143	5	9	−20078632448322012858575038616128389120
1	0	−19388482158833101439965554398357094 40	6	0	11017867156303922170994966093488560537 60
1	1	82082634558797623964730393945020825 60	6	1	66448257591532077766283921577139293388 80
1	2	−58416152172890170054809898875743109120	6	2	91707243321148816623080344491790644019 20
1	3	75842480167323819896585446551600496640	6	3	10296333530288664715204547691370134896640
1	4	−21077525184704167680567012539299266560 0	6	4	68432661104130985098442520438759227392 00
1	5	13618452579842393799840582494832820224 0	6	5	30303870749647325286759599375122012569 60
1	6	−19673380011295522174120502168095555584 0	6	6	91589743762221549435762204223557599232 0
1	7	79216590016681069471177813962164797440	6	7	23894725361988373019381098127642591232 0
1	8	−59859091103576645172144058190055751680	6	8	45054022158754454164122182527702794240
1	9	18326220317126356156222467072302796800	7	0	−18547794154773167570952844168523887411 20
1	10	−71088232016782885926676701594105958 40	7	1	−75390878244483868666802260780483451289 60
1	11	81571287194001841109712340528895232 0	7	2	−11455283520474845151288748928631759175 680
1	12	−36164138416078256404777989440207072 0	7	3	−10532811484287412546421885016991177113 600
1	13	−44637243978247300987553286056547600	7	4	−56288006517417259907496589607124860928 00
2	0	86456080550614125761731402791072563 20	7	5	−19617469100159521613348490588443167948 80
2	1	85585012335012951401718179340641894 40	7	6	−48046504342706830327161877584219734016 0
2	2	20812864432060921207062885690714882048 0	7	7	−81866144453011763538579483060810547200
2	3	25398307833670702694095833454451097600	8	0	23595008671949344321316102805346949529 60
2	4	60722076869598157944518397653617213440 0	8	1	79375595021541467809094180722688026214 40
2	5	19691331670165903708878704137721610240	8	2	10332903003270244092946854689083962163200
2	6	39175819448502844858690790991164805120	8	3	75338715286926309759745820069977915392 00
2	7	63917413426897278536630497852234137 60	8	4	31143329159556233140147352629829173248 00
2	8	51577861175147285247750616718405222400	8	5	80724627705295564521226347196075474944 0
2	9	62046070397789341001473301295673344 00	8	6	12553332885126071465731033212439756800 0
2	10	36404000712598792176707078109471436 80	9	0	−22688003992258932626447505840900197580 80
2	11	19830867920106764147066350151768217 60	9	1	−62328222727073441041582923254006284288 00
2	12	36755790923307571462766594603585248 0	9	2	−66055624630643581143474548861713776640 00
3	0	−39787816938051620059790474557930864640	9	3	−36360995468257636397629617863118553088 00
3	1	−15947607188980269310943489582040088576 0	9	4	−10715197653610977187060471233624670208 00
3	2	−73151401285592388620651077259524833280 0	9	5	−16437892663746066312631517891612639232 0
3	3	−78440076629316613711274817802972692480 0	10	0	16291230118299001487223932896448557875 20
3	4	−16775523936257798131863474374807912448 00	10	1	35451424852987259357067346033293184204 80
3	5	−66135385318438601399974086427690401792 0	10	2	28608958129335135818615988725513768140 80
3	6	−82734343836767481873416205036234473 4720	10	3	10817185458543789565367288495516889907 20
3	7	−81305279726239321202490323786504601600	10	4	17826154534659566866658191047674298368 0
3	8	−10588479528805288731987714993980375 0400	11	0	−84933496696144824007294956511988547584 0
3	9	−12330592804548067461951671658298572800	11	1	−13834401781290175138022060871740345548 80
3	10	−11075426977582842938551752217607413760	11	2	−76043669624697974234586489655035691008 0
3	11	−18281668831673599156007900331747840 00	11	3	−15290398393483494806917209185247559680 0
4	0	16046934538978432894252543433309683712 0	12	0	30461101443927662069726077043901202432 0
4	1	71622052501481861032681247296538542080 0	12	1	33281278480076599631643534570245062656 0
4	2	22530086578300309438653792090442432512 00	12	2	94874071276729045364882989890351923200
4	3	30051686911009457802401264355659218944 00	13	0	−67440944904415911980697770594884648960
4	4	36349186395885640248702704626333384704 00	13	1	−37465022666738942217557941148492759040
4	5	20392624486073050133423451163843991961 60	14	0	69769545652626487245757284679994572 80

where the bottom half of each matrix contains a binary generator matrix for the $[14, 13]$ and $[37, 35]$ tail-biting convolutional codes, respectively. If $\boldsymbol{B}_6$ denotes the generator matrix in [14, Eq. (13)], then the equivalences can be explicitly shown as

$$\boldsymbol{B}_6\boldsymbol{B}_6^{\mathrm{T}} = \frac{1}{2}\boldsymbol{U}_4\boldsymbol{B}_4\boldsymbol{B}_4^{\mathrm{T}}\boldsymbol{U}_4^{\mathrm{T}} = \frac{1}{2}\boldsymbol{U}_5\boldsymbol{B}_5\boldsymbol{B}_5^{\mathrm{T}}\boldsymbol{U}_5^{\mathrm{T}} \tag{87}$$

with

$$\boldsymbol{U}_4 = \begin{bmatrix} 2 & 1 & 1 & 0 & 0 & 1 & -2 & 0 & 0 & 0 & 0 & 0 \\ 1 & 0 & 0 & 0 & 0 & 0 & 0 & 0 & 0 & 0 & 0 & 0 \\ 2 & 1 & 1 & 0 & 0 & 2 & -3 & 1 & -1 & 1 & 0 & 0 \\ 0 & 0 & 0 & 1 & 0 & -1 & 1 & -1 & 1 & -1 & 0 & 0 \\ 2 & 2 & 1 & -1 & -1 & 2 & -4 & 2 & -1 & 1 & -1 & 1 \\ 2 & 2 & 1 & -1 & 0 & 2 & -4 & 2 & -1 & 1 & -1 & 1 \\ 2 & 2 & 0 & -1 & -1 & 2 & -4 & 3 & -1 & 1 & -1 & 1 \\ 0 & 0 & -1 & 0 & 0 & 0 & 0 & 0 & 0 & 0 & 0 & 0 \\ -1 & -1 & -1 & 0 & 0 & -2 & 2 & -1 & 1 & -1 & 1 & 0 \\ -1 & -1 & -1 & 0 & 0 & -1 & 2 & -1 & 1 & -1 & 1 & 0 \\ -1 & -1 & -1 & 1 & 0 & -2 & 3 & -2 & 2 & -1 & 1 & -1 \\ -2 & -3 & -1 & 2 & 1 & -4 & 6 & -5 & 3 & -2 & 2 & -1 \end{bmatrix}, \tag{88}$$

$$\boldsymbol{U}_5 = \begin{bmatrix} 1 & 0 & 0 & 0 & 0 & -1 & 0 & 0 & 0 & 0 & 0 & 0 \\ 1 & 0 & 0 & 0 & 0 & 0 & 0 & 0 & 0 & 0 & 0 & 0 \\ 0 & 0 & 0 & 0 & 0 & 0 & 0 & -1 & 0 & 1 & 0 & 0 \\ 1 & 0 & 0 & 0 & -1 & -1 & 0 & 1 & 0 & -1 & 0 & 0 \\ 1 & 1 & 0 & 0 & 0 & -1 & 0 & 1 & 0 & 0 & 0 & -1 \\ 0 & 0 & 0 & 0 & 0 & 0 & 0 & -1 & 0 & 0 & 0 & 1 \\ 0 & 0 & -1 & -1 & -1 & 0 & 1 & 0 & -1 & 0 & 0 & 1 \\ -1 & -2 & -1 & -1 & -2 & -1 & 2 & 0 & 0 & -2 & 0 & 2 \\ -1 & -2 & -1 & -1 & -2 & -1 & 1 & 0 & 0 & -2 & 1 & 2 \\ -1 & -2 & -1 & 0 & -2 & -1 & 1 & 0 & 0 & -2 & 1 & 2 \\ 0 & 1 & -1 & -1 & 1 & 1 & 0 & 0 & -1 & 2 & -1 & 0 \\ 0 & -1 & 0 & 0 & -1 & -1 & 0 & 0 & 1 & -1 & 0 & 1 \end{bmatrix}. \tag{89}$$

References

[1] J. H. Conway and N. J. A. Sloane, *Sphere Packings, Lattices and Groups*, 3rd ed. New York, NY: Springer, 1999. [Online]. Available: https://doi.org/10.1007/978-1-4757-6568-7

[2] G. D. Forney, Jr. and L.-F. Wei, "Multidimensional constellations—part I: Introduction, figures of merit, and generalized cross constellations," *IEEE J. Sel. Areas Commun.*, vol. 7, no. 6, pp. 877–892, Aug. 1989. [Online]. Available: https://doi.org/10.1109/49.29611

[3] G. D. Forney, Jr., "Multidimensional constellations—part II: Voronoi constellations," *IEEE J. Sel. Areas Commun.*, vol. 7, no. 6, pp. 941–958, Aug. 1989. [Online]. Available: https://doi.org/10.1109/49.29616

[4] Q. Guo, T. Johansson, and P. Stankovski, "Coded-BKW: solving LWE using lattice codes," in *Proc. Annual Cryptology Conference (CRYPTO)*, 2015, pp. 23–42. [Online]. Available: https://doi.org/10.1007/978-3-662-47989-6_2

[5] A. Sablayrolles, M. Douze, C. Schmid, and H. Jégou, "Spreading vectors for similarity search," in *Proc. Int. Conf. Learning Representations*, New Orleans, LA, May 2019. [Online]. Available: https://openreview.net/forum?id=SkGuG2R5tm

[6] B. Allen, "Optimal template banks," *Phys. Rev. D*, vol. 104, p. 042005, Aug. 2021. [Online]. Available: https://doi.org/10.1103/PhysRevD.104.042005

[7] R. M. Gray and D. L. Neuhoff, "Quantization," *IEEE Trans. Inf. Theory*, vol. 44, no. 6, pp. 2325–2383, Oct. 1998. [Online]. Available: https://doi.org/10.1109/18.720541

[8] R. Zamir, *Lattice Coding for Signals and Networks*. Cambridge, UK: Cambridge University Press, 2014. [Online]. Available: https://doi.org/10.1017/CBO9781139045520

[9] A. Gersho, "Asymptotically optimal block quantization," *IEEE Trans. Inf. Theory*, vol. IT-25, no. 4, pp. 373–380, July 1979. [Online]. Available: https://doi.org/10.1109/TIT.1979.1056067

[10] L. Fejes Tóth, "Sur la représentation d'une population infinie par un nombre fini d'éléments," *Acta Mathematica Hungarica*, vol. 10, no. 3–4, pp. 299–304, Sept. 1959, in French. [Online]. Available: https://doi.org/10.1007/bf02024494

[11] E. S. Barnes and N. J. A. Sloane, "The optimal lattice quantizer in three dimensions," *SIAM J. Alg. Disc. Meth.*, vol. 4, no. 1, pp. 30–41, Mar. 1983. [Online]. Available: https://doi.org/10.1137/0604005

[12] J. H. Conway and N. J. A. Sloane, "On the Voronoi regions of certain lattices," *SIAM J. Alg. Disc. Meth.*, vol. 5, no. 3, pp. 294–305, Sept. 1984. [Online]. Available: https://doi.org/10.1137/0605031

[13] B. D. Kudryashov and K. V. Yurkov, "Near-optimum low-complexity lattice quantization," in *2010 IEEE International Symposium on Information Theory*, 2010, pp. 1032–1036. [Online]. Available: https://doi.org/10.1109/ISIT.2010.5513730

[14] E. Agrell, D. Pook-Kolb, and B. Allen, "Glued lattices are better quantizers than K_{12}," *IEEE Trans. Inf. Theory*, vol. 70, no. 11, pp. 8414–8418, Nov. 2024. [Online]. Available: https://doi.org/10.1109/TIT.2024.3398421

[15] E. Agrell and B. Allen, "On the best lattice quantizers," *IEEE Trans. Inf. Theory*, vol. 69, no. 12, pp. 7650–7658, Dec. 2023. [Online]. Available: https://doi.org/10.1109/TIT.2023.3291313

[16] D. Pook-Kolb, B. Allen, and E. Agrell, "Exact calculation of quantizer constants for arbitrary lattices," *Beijing Journal of Pure and Applied Mathematics*, vol. 3, no. 1, pp. 67–120, 2026. [Online]. Available: https://doi.org/10.4310/BPAM.250918173055

[17] S. Lyu, Z. Wang, C. Ling, and H. Chen, "Better lattice quantizers constructed from complex integers," *IEEE Trans. Commun.*, vol. 70, no. 12, pp. 7932–7940, Dec. 2022. [Online]. Available: https://doi.org/10.1109/TCOMM.2022.3215685

[18] E. Agrell and T. Eriksson, "Optimization of lattices for quantization," *IEEE Trans. Inf. Theory*, vol. 44, no. 5, pp. 1814–1828, Sept. 1998. [Online]. Available: https://doi.org/10.1109/18.705561

[19] N. J. A. Sloane, personal communication, Feb. 1998.

[20] B. Allen and E. Agrell, "The optimal lattice quantizer in nine dimensions," *Annalen der Physik*, vol. 533, no. 12, p. 2100259, Dec. 2021. [Online]. Available: https://doi.org/10.1002/andp.202100259

[21] E. Agrell, D. Pook-Kolb, and B. Allen, "Optimization and identification of lattice quantizers," *IEEE Trans. Inf. Theory*, vol. 71, no. 8, pp. 6490–6501, 2025. [Online]. Available: https://doi.org/10.1109/TIT.2025.3565218

[22] R. Zamir and M. Feder, "On lattice quantization noise," *IEEE Trans. Inf. Theory*, vol. 42, no. 4, pp. 1152–1159, July 1996. [Online]. Available: https://doi.org/10.1109/18.508838

[23] J. H. Conway and N. J. A. Sloane, "On the enumeration of lattices of determinant one," *Journal of Number Theory*, vol. 15, no. 1, pp. 83–94, Aug. 1982. [Online]. Available: https://doi.org/10.1016/0022-314X(82)90084-1

[24] D. Pook-Kolb, E. Agrell, and B. Allen, "The Voronoi region of the Barnes–Wall lattice Λ_{16}," *IEEE J. Sel. Areas Inf. Theory*, vol. 4, pp. 16–23, 2023. [Online]. Available: https://doi.org/10.1109/JSAIT.2023.3276897

[25] A. Gersho and R. M. Gray, *Vector Quantization and Signal Compression*. Boston, MA, USA: Kluwer Academic Publishers, 1992. [Online]. Available: doi.org/10.1007/978-1-4615-3626-0

[26] J. Martinet, *Perfect Lattices in Euclidean Spaces*, ser. Grundlehren der mathematischen Wissenschaften. Berlin, Germany: Springer-Verlag, 2003, no. 327. [Online]. Available: https://doi.org/10.1007/978-3-662-05167-2

[27] B. Souvignier, "Irreducible finite integral matrix groups of degree 8 and 10," *Mathematics of Computation*, vol. 63, no. 207, pp. 335–350, 1994. [Online]. Available: http://www.jstor.org/stable/2153579

[28] G. Nebe and N. Sloane, "A catalogue of lattices," accessed: 2024-07-30. [Online]. Available: http://www.math.rwth-aachen.de/~Gabriele.Nebe/LATTICES/

[29] The GAP Group, "GAP – Groups, Algorithms, and Programming, Version 4.12dev." [Online]. Available: https://www.gap-system.org

[30] M. Dutour Sikirić, A. Schürmann, and F. Vallentin, "A generalization of Voronoi's reduction theory and its application," *Duke Mathematical Journal*, vol. 142, no. 1, pp. 127–164, Mar. 2008. [Online]. Available: https://doi.org/10.1215/00127094-2008-003